SANDIA REPORT
SAND2014-0626
Unlimited Release
Printed January 2014

Theoretical Foundation for Measuring the Groundwater Age Distribution

W. Payton Gardner and Bill W. Arnold

Prepared by
Sandia National Laboratories
Albuquerque, New Mexico 87185 and Livermore, California 94550

Sandia National Laboratories is a multi-program laboratory managed and operated by Sandia Corporation, a wholly owned subsidiary of Lockheed Martin Corporation, for the U.S. Department of Energy's National Nuclear Security Administration under contract DE-AC04-94AL85000.

Sandia National Laboratories

Issued by Sandia National Laboratories, operated for the United States Department of Energy by Sandia Corporation.

Printed in the United States of America. This report has been reproduced directly from the best available copy.

Available to DOE and DOE contractors from
U.S. Department of Energy
Office of Scientific and Technical Information
P.O. Box 62
Oak Ridge, TN 37831

Telephone: (865) 576-8401
Facsimile: (865) 576-5728
E-Mail: reports@adonis.osti.gov
Online ordering: http://www.osti.gov/bridge

Available to the public from
U.S. Department of Commerce
National Technical Information Service
5285 Port Royal Rd.
Springfield, VA 22161

Telephone: (800) 553-6847
Facsimile: (703) 605-6900
E-Mail: orders@ntis.fedworld.gov
Online order: http://www.ntis.gov/help/ordermethods.asp?loc=7-4-0#online

SAND2014-0626
Unlimited Release
Printed January
2014

Theoretical Foundation for Measuring the Groundwater Age Distribution

W. Payton Gardner and Bill W. Arnold
Advanced Systems Analysis and Research
Sandia National Laboratories
P.O. Box 5800
Albuquerque, New Mexico 87185-MS0747

Abstract

In this study, we use PFLOTRAN, a highly scalable, parallel, flow and reactive transport code to simulate the concentrations of ^{3}H, ^{3}He, CFC-11, CFC-12, CFC-113, SF_6, ^{39}Ar, ^{81}Kr, ^{4}He and the mean groundwater age in heterogeneous fields on grids with an excess of 10 million nodes. We utilize this computational platform to simulate the concentration of multiple tracers in high-resolution, heterogeneous 2-D and 3-D domains, and calculate tracer-derived ages. Tracer-derived ages show systematic biases toward younger ages when the groundwater age distribution contains water older than the maximum tracer age. The deviation of the tracer-derived age distribution from the true groundwater age distribution increases with increasing heterogeneity of the system. However, the effect of heterogeneity is diminished as the mean travel time gets closer the tracer age limit. Age distributions in 3-D domains differ significantly from 2-D domains. 3D simulations show decreased mean age, and less variance in age distribution for identical heterogeneity statistics. High-performance computing allows for investigation of tracer and groundwater age systematics in high-resolution domains, providing a platform for understanding and utilizing environmental tracer and groundwater age information in heterogeneous 3-D systems.

Groundwater environmental tracers can provide important constraints for the calibration of groundwater flow models. Direct simulation of environmental tracer concentrations in models has the additional advantage of avoiding assumptions associated with using calculated groundwater age values. This study quantifies model uncertainty reduction resulting from the addition of environmental tracer concentration data. The analysis uses a synthetic heterogeneous aquifer and the calibration of a flow and transport model using the pilot point method. Results indicate a significant reduction in the uncertainty in permeability with the addition of environmental tracer data, relative to the use of hydraulic measurements alone. Anthropogenic tracers and their decay products, such as CFC11, ^{3}H, and ^{3}He, provide significant constraint on input permeability values in the model. Tracer data for ^{39}Ar provide even more complete

information on the heterogeneity of permeability and variability in the flow system than the anthropogenic tracers, leading to greater parameter uncertainty reduction.

CONTENTS

FIGURES

TABLES

1. INTRODUCTION

Environmental tracers occur ubiquitously as non-applied chemical and isotopic species that provide valuable information on groundwater age, velocity, recharge conditions and the location of groundwater discharge. Methods of tracer interpretation range in their treatment of transport from a simplified black box (e.g. lumped parameter models) to numerical models of reactive flow and transport. Computational demand has limited current studies that interpret environmental tracer concentrations. We use PFLOTRAN a massively parallel flow and reactive transport code to simulate multiple tracer concentrations directly. This new capability is then leveraged to explore the distribution of tracer concentrations and tracer-derived ages in high-resolution 2-D and 3-D heterogeneous systems. We show that simulation of many tracer species in high-resolution, three-dimensional heterogeneous domains is possible. We report on simulations with meshes over 10 million nodes, and simulation time periods over 100,000 years, which can be run with wall clock times less than two hours when spread over 800 processors. The highly linear scaling performance of PFLOTRAN implies that even larger meshes can be run within reasonable times by advancing to larger computational platforms. Significant heterogeneity exists in the spatial distribution of mean age even in relatively homogenous domains after flow path lengths 25 times the spatial correlation length. Tracer-derived ages show systematic biases toward younger ages when the groundwater age distribution contains water older than the maximum tracer age. The addition of the third dimension increases connectivity by adding another degree of freedom for groundwater flow. Mean age and spatial variance in age is decreased in 3-D systems relative to 2-D systems.

In contrast to other studies to date, our technique is to directly simulate the environmental tracer concentration, which is the direct observation made in a groundwater sample. We use this capability to quantify the reduction in uncertainty in parameter estimation when environmental tracer information is added to the inversion. Groundwater models are often under constrained by hydrologic data alone, causing non-unique parameter estimates and significant uncertainty in model parameters and predictions, particularly regarding contaminant transport. Here we created a synthetic data set of pressure and chemistry from a heterogeneous aquifer. We then conduct a pilot point permeability field calibration against the synthetic data using pressure alone and pressure and environmental tracer concentrations using PFLOTRAN coupled the PEST parameter estimation and uncertainty quantification suite. We calculate the 95% linear confidence intervals of the pilot point permeability estimates for each inversion. Adding tracer data into the inversion reduces the uncertainty in permeability estimates by orders of magnitude, drastically improving our estimates of subsurface parameters. This study demonstrates the effectiveness of directly simulating environmental tracer concentrations in a high-resolution groundwater flow and transport model in the calibration process. With this approach the model directly matches the collected data, effectively bypassing potentially questionable assumptions associated with the calculation of groundwater age from tracer concentrations.

As a result of this study we have significantly improved the simulation capabilities of environmental tracers in high-resolution 2-D and 3-D domains. By simulating tracer concentration directly our technique will allow quantitative interpretation of environmental tracers in dual continuum, non-isothermal, dual-phase and mechanically deforming situations. In addition, the data observed and measured in the field (i.e. concentration) can be directly used in parameter estimation, calibration and prediction. This data is shown to have considerable power in improved subsurface parameter estimates. These results suggest that future studies that consider subsurface flow and transport problems should include measurements of several environmental tracer concentrations and that the collection of this data will significantly improve site characterization and subsequent predictions.

2. HIGH PERFORMANCE SIMULATION OF ENVIRONMENTAL TRACERS IN HETEROGENEOUS DOMAINS.

Computational demand has limited current studies that interpret environmental tracer concentrations. To date, studies that do include a full treatment of the transport process have been confined to particle tracking, and have been limited in dimensionality and/or number of tracers simulated. To maximize the information contained in tracer concentrations, interpretation methods should include full consideration of all the transport processes for many tracers in three dimensions.

A common use of environmental tracers is to assess the apparent age of groundwater samples. Groundwater samples are not composed of water of a single age, but an age distribution and the environmental tracer concentration at the sampling point is a function of that distribution (Cornaton & Perrochet 2006a, Cornaton & Perrochet 2006b, Maloszewski & Zuber 1996, Varni & Carrerra 1998). Different groundwater age distributions will lead to different mean ages for a given tracer concentration (e.g. Gardner et al. 2011, Solomon et al. 2010). The use of multiple tracers can help reduce the uncertainty in the most applicable age distribution (Gardner et al. 2011, Solomon et al. 2010). In order to better characterize the age distribution in a heterogeneous flow system it is clear that many tracers with age information over many different time scales needs to be interpreted (McCallum et al. 2013).

The groundwater age distribution by itself is useful for building conceptual models of a flow system; however, in order to use this information to improve quantitative predictive capability of groundwater flow and transport models, the tracer information must be incorporated into a numerical model. Groundwater mean age can be modeled using the advection-dispersion equation (Goode 1996), and tracer-derived ages can be used to help constrain groundwater models (Murphy et al. 2011, Plummer et al. 2004, Portniaguine & Solomon 1998, Sanford 2011, Sanford et al. 2004). Mean groundwater age is generally modeled, and then compared to the apparent mean age determined by a single tracer concentration assuming piston flow (Murphy et al. 2011, Plummer et al. 2004, Portniaguine & Solomon 1998, Sanford 2011, Sanford et al. 2004).

The comparison of modeled and tracer-derived age requires a significant assumption about the age distribution in the groundwater sample. The tracer-derived mean age may not be equal to the groundwater mean age. Heterogeneity can cause significant bias in the tracer-derived age due to the truncation of age information (McCallum et al. 2013, Weissmann et al. 2002).
In heterogeneous, transient systems, the groundwater age distribution is complex and can change with time (Troldborg et al. 2008). Thus, matching tracer concentration provides better information (Troldborg et al. 2008). The travel time distribution can be simulated at a point using particle tracking and the expected tracer concentration calculated using the convolution of the age distribution and the tracer input function (McCallum et al. 2013, Troldborg et al. 2008). However, in order to investigate the spatial distribution particles must be tracked at each point on the model domain.

In this section, we use PFLOTRAN a massively parallel flow and reactive transport code to simulate multiple tracer concentrations with transport information over many time scales (Hammond et al. 2012). We show that this computational platform is capable of simulating the concentration for many tracers in high-resolution, three-dimensional, heterogeneous domains. We use this capability to explore the distribution of tracer concentrations and tracer-derived ages in high-resolution 2-D and 3-D heterogeneous systems. The use of massively parallel flow and transport codes opens up a new suite of tools for utilizing environmental tracer concentrations in understanding hydrologic systems. Taking advantage of modern computational power allows for unprecedented exploration of the systematics of environmental tracer concentrations and derived ages in complex systems, and the proper use of these tracers to understand hydrologic systems dynamics.

2.1 Numerical Methods

In this study we use PFLOTRAN, a scalable, parallel, multi-phase, multi-component, non-isothermal reactive flow and transport code to simulate multiple environmental tracer concentrations in heterogeneous 2-D and 3-D domains. For all simulations in this paper, PFLOTRAN was run in the Richard's equation mode, which simulates variably saturated single-phase flow and transport.

PFLOTRAN solves the advection dispersion equation using fully implicit, integral finite volume technique. Operator splitting is used to handle the disparity in time scales between flow and transport. PFLOTRAN is written in object oriented FORTRAN 9X and 2003. The Message Passing Interface is used to allow for scalable, distributed-memory parallelism. PFLOTRAN uses an efficient domain-decomposition paradigm for distributing the computational burden across processors on both structured and unstructured grids. The Portable Extensible Toolkit for Scientific Computation (PETSc) library is leveraged to provide access to cutting edge parallel Newton-Krylov solvers. PFLOTRAN is designed from the ground up to utilize parallel IO with the HDF5 file format. PFLOTRAN is open source, can be employed on a variety of architectures, and is fully scalable from single processor laptops to over 2^{17} core peta-scale simulations (Hammond et al. 2012).

Boundary conditions for the environmental tracers were assigned as time-dependent prescribed concentrations derived the atmospheric concentration history for a given tracer. For simplification, dissolved gas tracer concentration at recharge was calculated assuming a recharge temperature of 25 C, 1 atmosphere of pressure and no addition of excess air. However, PFLOTRAN could calculate aqueous concentrations given the atmospheric concentration and temperature using temperature dependent Henry's coefficients if the proper species and solubilities were input into the PFLOTRAN geochemical database.

Decay and ingrowth of radioisotope tracers was handled with user-defined reactions. Decay constants for ^{3}H, ^{39}Ar and ^{81}Kr were taken from Cook & Herczeg (2000). The in-growth rate of ^{4}He was calculated assuming average crustal U and Th concentrations, and complete loss of radiogenic ^{4}He from the mineral grains. Subsurface production of ^{3}He, ^{39}Ar and SF_6 were neglected; however, these reactions could be considered in future simulations. All tracers were assumed to be non-sorbing and chemically inert which is reasonable for these tracers (Cook & Herczeg 2000).

2.1.1 Two Dimensional Heterogeneous Confined Aquifer:

One of the primary benefits of the high-resolution, numerical simulation of multiple tracer species is the ability to investigate the effect of heterogeneity on the modeled tracer concentrations, tracer-derived ages, and the "true" modeled mean age of the groundwater. Here we use Sequential Gaussian Simulation to create stochastic, heterogeneous permeability fields. Here we consider steady state flow in 500 m by 500 m 2-D domain, gridded with 1 m by 1m grid blocks. Constant head boundary conditions were applied on the east and west boundaries to give a head gradient of 0.01 m/m. The top, bottom, north and south faces were considered to be no flow boundaries. Historical tracer concentrations were applied at the west boundary. The simulations were carried out in two steps. The first step was to model "pre-modern" conditions by running simulations with pre-anthropogenic boundary conditions for over 100,000 years allowing the mean age and ^{39}Ar to come to equilibrium. The model was then restarted with finer time stepping in order to allow for the application of the "modern" anthropogenic boundary conditions over the past 70 years.

For the first set of simulations, the seed data for the sequential Gaussian simulation were taken from a lognormal distribution of permeabilites with a mean of $1x10^{-13}m^2$ and one or two orders of magnitude standard deviation. Arbitrary spatial correlation lengths of 20 m in the *y* (north-south) direction and 20 m in the *x* (east-west) direction and 20 m in the z (3-D only) were chosen. The 2-D simulated, unconditional permeability field is shown in Figure 1. In order to isolate the effect of heterogeneity in permeability, porosity was assigned as constant across the domain.

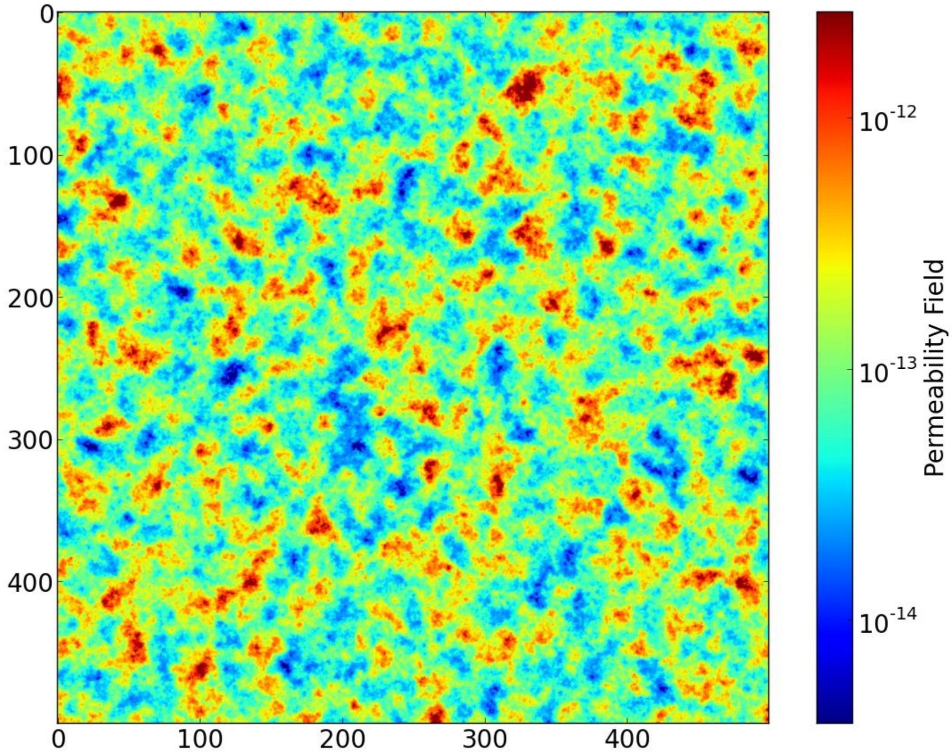

Figure 1 - Simulated unconditional permeability distribution – values are m^2 intrinsic permeability. Units on the x and y-axis are the distance in each direction in meters.

The "apparent" age can be calculated for each tracer using the simulated concentration and the appropriate "piston-flow" age equation for each tracer. The calculation of these apparent ages from the simulated concentration is different for each tracer; for a detailed explanation of the age calculation for each tracer, see Cook & Herczeg 2000). Tracer-derived ages are compared to the modeled mean groundwater age using (Goode 1996):

$$\frac{\partial A\varphi\rho}{\partial t} = \varphi\rho - \nabla \cdot A\rho q_w + \nabla \cdot \varphi\rho D \cdot \nabla A + Q_A. \tag{1}$$

Where q_w is the groundwater flux, $Q_A$is a generic source or sink of age, and A is the mean residence time for a mixture of groundwater defined by Goode 1996 and Spalding 1958:

$$A = \frac{\int_0^\infty tc\ dt}{\int_0^\infty c\ dt} \tag{2}$$

Where c is the "concentration" of groundwater of a given age. Equation 2 states that the mean age of the groundwater is analogous to a conservative solute concentration, and is given by the mass-weighted average age of the mixed groundwater. It is important to note that our model

produces the mean residence time of groundwater for each cell in the model, which is in fact only the first moment of the groundwater age distribution for that particular element.
Given the time varying boundary conditions, analytical detection limits and sampling error, every "age" tracer has limits to its range of applicability. In this study, we apply characteristic age ranges for all tracers (Table 1). For CFC's and SF_6, early time age ranges are set based on the beginning of their observable anthropogenic increase in concentration giving maximum ages around 60 and 50 years respectively (Table 1). The peak in atmospheric concentration gives the minimum age for CFC's: 1994 for CFC-11, 2000 for CFC-12, and 1996 for CFC-113. $^3H/^3He$ maximum age is set to 75 years, the time it takes for a pre-modern ^3H concentration of 6 TU to decay to 0.1 TU, which is a representative background level (Kaufman & Libby 1954). The maximum age for ^{39}Ar is set to 1000 years that is around 3 half-lives and the minimum age is set 100 years which 1/3 of a half-life. These age ranges are not absolute, but are reasonable for the purposes of this investigation.

Table 1 - Representative age ranges for environmental tracers simulated in this study.

Tracer	Minimum Age	Maximum Age
3H/3He	0	75
CFC-11	18	60
CFC-12	12	60
CFC-113	16	60
SF6	0	50
39Ar	100	1000

2.1.2. High Fidelity 3-D Simulation of Multiple Environmental Tracers:

A massively parallel approach provides the ability to simulate tracer concentration in high-resolution, heterogeneous, 3-D domains. To facilitate comparison between 2-D and 3-D results, we simulate a 500 m x 500 m confined aquifer with a thickness of 50 m gridded with 1 m x 1m x 1m grid blocks. Boundary conditions are identical to the two dimensional case with no flow and no transport boundaries on the top, bottom, north and south faces of the aquifer. Constant head boundary conditions which provide a gradient of 0.01 m/m with flow from west to east are applied on the east and west faces. As was done for the 2-D experiment, the 3-D simulations were carried out in two steps. Initially, constant concentration boundary conditions of average pre-modern atmospheric equilibrium were applied to the west boundary and the simulation was run for 10^6 years in order to reach steady state conditions. The model was then restarted and the historical, anthropogenic atmospheric concentrations over the last 100 years were applied on the west boundary. A zero concentration gradient was applied at the east face of the aquifer. Random, heterogeneous permeability fields were created with sequential Gaussian simulation as in the 2-D simulations. The permeability seed data for the sequential Gaussian simulation were sampled from a lognormal distribution with a mean permeability of $1x10^{-13}$ m ^{2} and 1 order or 2 orders of magnitude standard deviation. Correlation lengths were set to 20 m in the y-direction, 20 m in the x-direction and 20 m in z. As in the 2-D case, a constant porosity was assigned throughout the domain.

2.2 Results

A significant difference in this study to previous studies on the effect of heterogeneity on groundwater age is that we solve the advection dispersion equation at all points in the domain, and can investigate the spatial distribution of concentration and mean groundwater age. Thus, we report on the spatial distribution of mean age, rather than the distribution of age a single point as produced by the particle tracking methods of McCallum et al. (2013) and Weissmann et al. (2002).

2.2.1. 2-D simulations:

Figure 2 shows the distribution of modeled mean age (A_m) less than 100 years and tracer-derived apparent age (A_{tr}) for the young tracers. Given the age limits of the young tracers, they provide age information only in the first 200 m or so. Within the first 200 m, the maximum age of the water is limited by the max age for the tracer, thus fingers of water which have a maximum mean age over 100 years can only be interpreted as older than the maximum age of the particular tracer. . There are subtle differences in the quality of match between the young tracers. CFC-12 appears to match the early portions of the flow path better, while $^3H/^3He$ shows the best match to the actual mean age at longer flow paths due to a wider age range. The spatial distribution of age derived from tracers has limited resolution and halos of excess apparent age exist around fingers of old water. The loss of age resolution is caused by analytical error and/or dating method limitations, for example using the mean annual concentration of CFC or SF_6 limits the smallest time increment to one year. $^3H/^3He$ ages appear to have less resolution than CFC-12 early in the flow path, which is probably due to dispersive smearing of the sharp peaks ^3H input function. The halo effect will increase when sampling and analytical error increase.

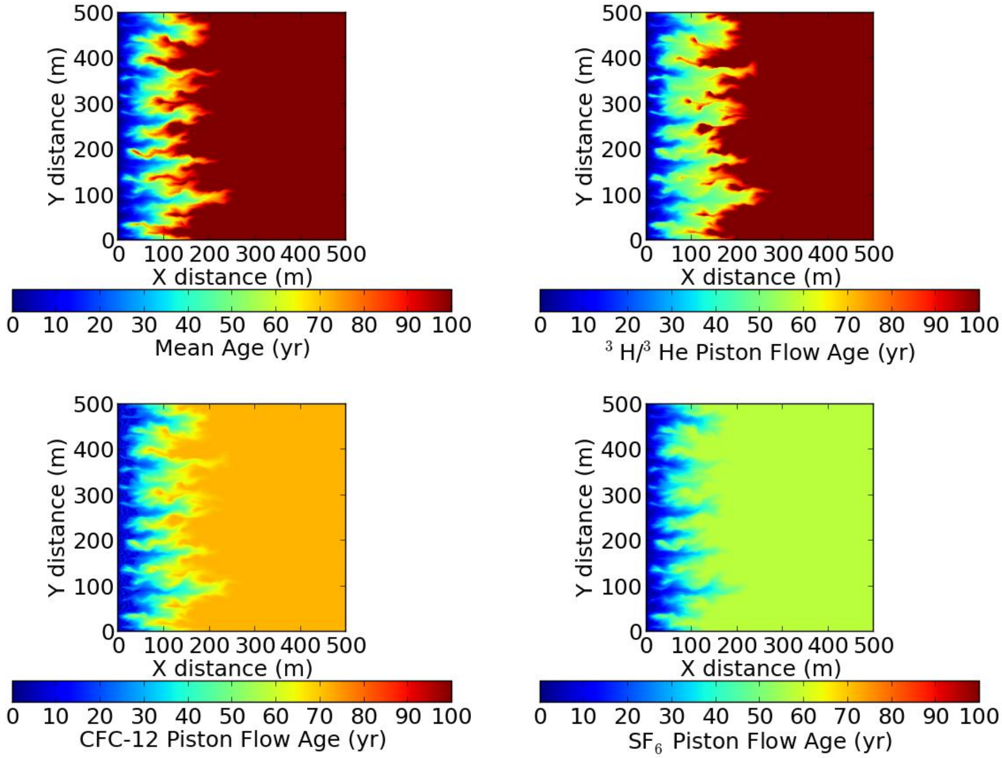

Figure 2 - Simulated mean groundwater age and tracer-derived ages for young tracers: $^3H/^3He$, CFC-12, and SF_6.

The full spatial distribution of mean age and the ^{39}Ar derived apparent age is given in Figure 3. The spatial mean age distribution shows significant heterogeneity even at the end of the 500 m flow path, which is 25 times the spatial correlation length. After 100 m, ages enter the ^{39}Ar dating range and the spatial distribution of ^{39}Ar apparent age matches the mean modeled age well. The quality of the match between ^{39}Ar apparent age and modeled mean age is primarily due to the fact that ^{39}Ar has a large age range which completely spans the mean age distribution in this reservoir at flow paths lengths greater than 100 m. Without prior knowledge of the heterogeneity structure and/or groundwater velocity in the reservoir, it would be hard to predict at what points along the flow path ^{39}Ar would give the best information. As flow paths increase, larger age distributions should be expected providing impetus for multi-tracer sampling campaigns.

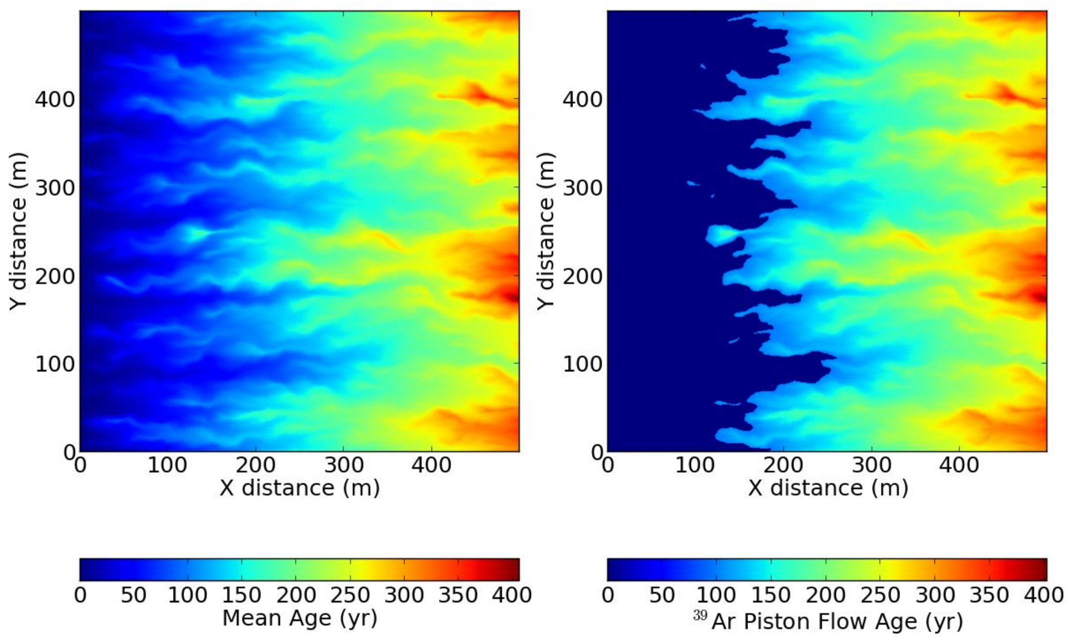

Figure 3 - Simulated mean age for the full age range and the ^{39}Ar apparent age distribution.

The average of the modeled spatial mean age ($\bar{A}_m$) and tracer-derived apparent age ($\bar{A}_{tr}$) for y-z planes with increasing distance along the flow path (X) are compared in upper plot in Figure 4. The average apparent age for CFC-12 early in the flow path is much larger than the true mean groundwater age. This artifact is due to inability to distinguish waters younger than the peak concentration of CFC-12 adding artificial age to those waters. SF_6 shows a muted but similar trend to CFC-12; however, the increase in SF_6 age at early times is not due to a minimum age limit, rather the limit in age resolution of SF_6 which is relatively large compared to the mean age early in the flow path. ^{3}H/^{3}He mean ages are close the true average modeled mean age at early distances. For all three young tracers, the tracer-derived mean age becomes less than the modeled mean age as the flow path increases due to age truncation. However, $\bar{A}_{tr}$ from the young tracers is still indicative of $\bar{A}_m$ for flow distances up to about 200 m. ^{39}Ar provides no age information until the flow path length is greater than 100 m, after this point the ^{39}Ar mean age tracks the modeled mean age well.

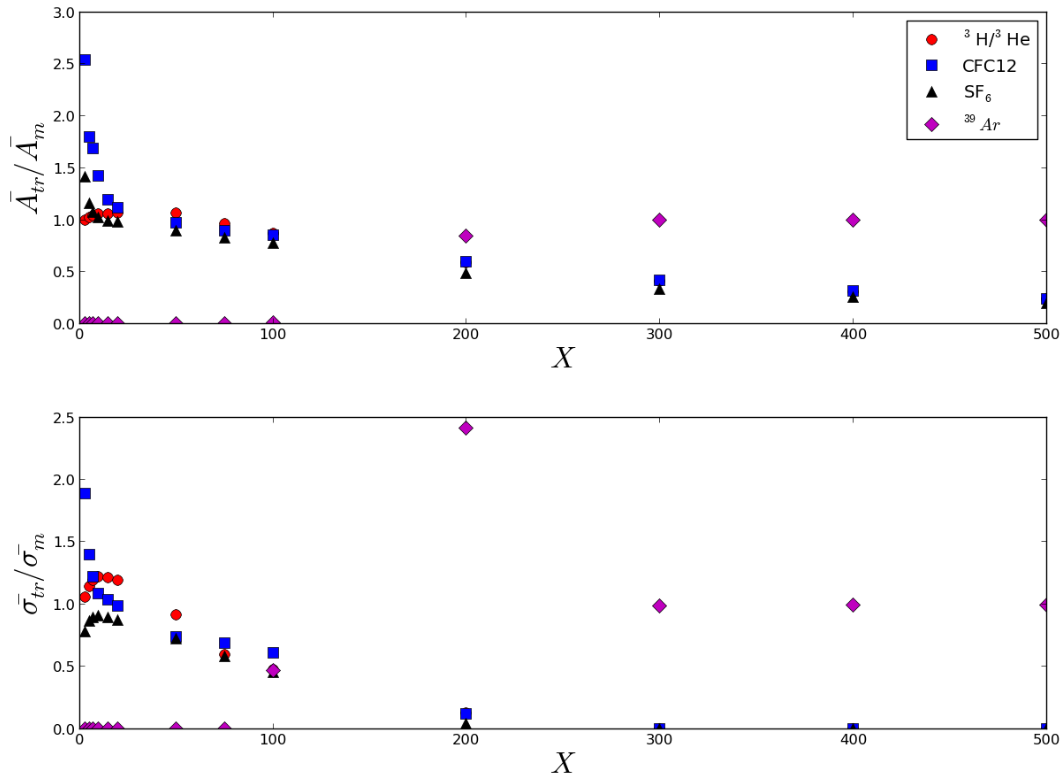

Figure 4 - Average tracer-derived age ($\bar{A}_{tr}$ - top) and standard deviation ($\bar{\sigma}_{tr}$ - bottom) for age distributions in y-z planes at increasing flow path length (*X*) normalized by average ($\bar{A}_m$) and standard deviation ($\bar{\sigma}_m$) of the modeled mean age distribution. Triangles, squares, circles and diamonds are the moments derived from SF_6, CFC-12, $^3H/^3He$ and ^{39}Ar concentrations respectively.

The lower plot in Figure 4 gives a comparison of the variation (given as the standard deviation) in the spatial age distribution ($\bar{\sigma}_{tr}$) within the y-z plane for tracer-derived apparent ages and modeled groundwater mean age ($\bar{\sigma}_m$). CFC-12 variance is greater than the variance in modeled mean age at short flow distances due to minimum age limit, while variation SF_6 and $^3H/^3He$ remains close to the modeled mean age variance up to flow distances of 50 m. The variance in young-tracer age distribution falls rapidly compared to the modeled mean age variance with increasing flow distance. Thus, it appears $\bar{\sigma}_{tr}$ is less robust than $\bar{A}_{tr}$ to age truncation limitations. ^{39}Ar variance is null until water begins to reach the minimum age limit, where it spikes artificially due to the large difference between the datable water and water assigned a zero age due to the minimum age limit. At distances over 300 m, $\bar{\sigma}_{tr}$ derived from ^{39}Ar matches $\bar{\sigma}_m$ as the ^{39}Ar age range completely spans the mean age distribution in reservoir in this area.
The effect of the degree of heterogeneity on the spatial distribution of tracer-derived age and modeled mean age was investigated by increasing the lognormal variance of the permeability distribution to two orders of magnitude keeping all other heterogeneity parameters constant. Figure 5 shows $\bar{A}_{tr}$ for the three young tracers normalized by $\bar{A}_m$ for y-z planes at increasing x distance for lognormal standard deviations of 1 and 2 orders of magnitude. In general, $\bar{A}_{tr}$

shows increased bias toward younger ages early in the flow path (lower $\bar{A}_{tr}/\bar{A}_m$ ratios) when the degree of heterogeneity is increased - consistent with McCallum et al. (2013). However, we show that the effect of heterogeneity on the age bias decreases with distance down the flow path. It is also apparent that the spatial variance in age derived from tracers is underestimated when compared to the true variance. Truncation of age information from tracers limits the span of ages to the maximum tracer age, thus reducing the variance in the spatial age distribution. In addition, the degree of underestimation in age-variance is greater when the heterogeneity is increased (lower plot Figure 5). Similar to the mean age bias, the effect of greater heterogeneity on the underestimation of age-variance decreases as the flow path length increases (lower plot Figure 5).

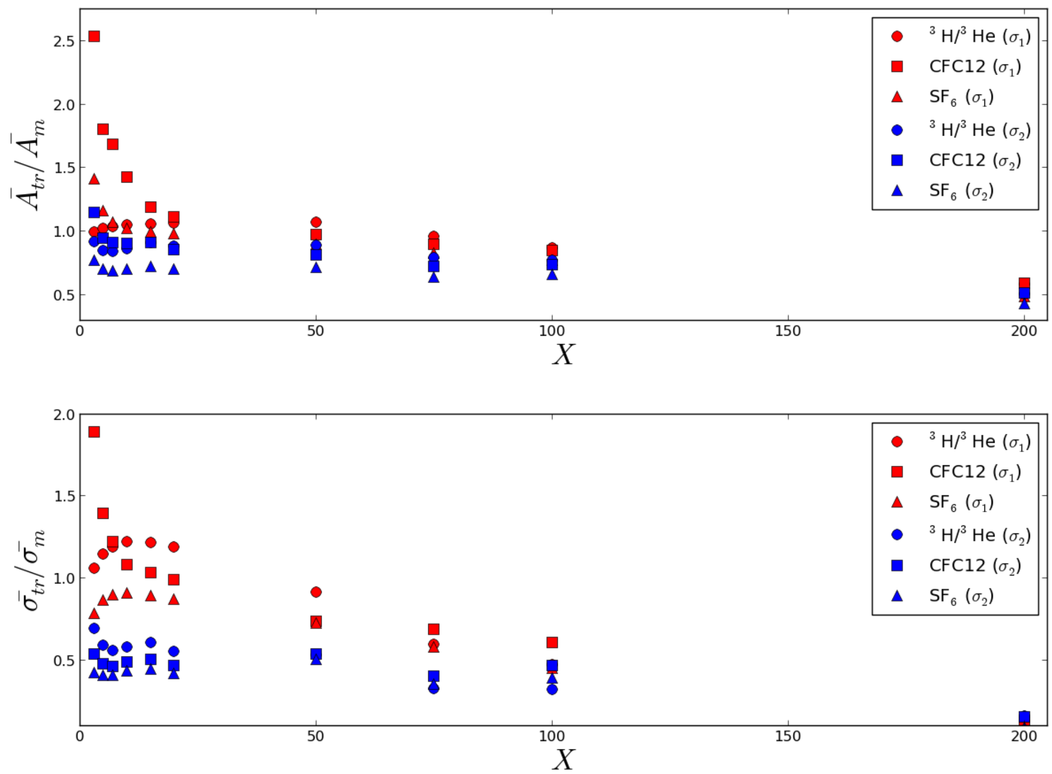

Figure 5 - Average tracer-derived apparent age ($\bar{A}_{tr}$) and standard deviation ($\bar{\sigma}_{tr}$) for spatial age distributions in *y-z* planes normalized by average modeled mean age ($\bar{A}_m$) and standard deviation of the modeled mean age ($\bar{\sigma}_m$) distribution as flow path distance increases for the 2-D case. Values plotted for lognormal heterogeneous permeability fields with one (σ_1) and two (σ_2) orders of magnitude log normal standard deviations.

2.2.2. 3-D Simulations:

In this section we extend the 2-D by adding the 3rd dimension. Here we report on high-fidelity simulations with around 10 million elements, distributed across ~10^3 processors. The scalability of PFLOTRAN allows for much larger simulations distributed across greater than of 10^5 processors; however, we restrict ourselves to smaller simulations as it suits the purpose of this paper, allows for reduced time in the scheduling queue, and reduces the mass-storage overhead associated with large 3-D data files.

The average tracer ages ($\bar{A}_{tr}$) and standard deviation ($\bar{\sigma}_{tr}$) for y-z planes show similar biases with increasing x-distance as the 2-D case when the heterogeneity field has one order of magnitude standard deviation (Figure 6). Mean age is artificially overestimated early in the flow path for CFC-12 and SF_6 and increasingly underestimated as the flow path length increases similar to the 2-D case. The mean age over estimation at short distances is higher in the 3-D case than the 2-D case. Additionally, the ^{39}Ar-derived age does not match the modeled mean age until farther along the flow path (flow path lengths over 300 m compared to 200 m in the 2-D case). Increasing the degree of heterogeneity from one order magnitude to two orders of magnitude lognormal standard deviation in the 3-D field causes similar effects on the tracer-derived age distribution to the 2-D case. Here $\bar{A}_{tr}$ shows increased bias toward younger ages and variance in tracer-derived age is increasingly underestimated when the heterogeneity increases (Figure 7).

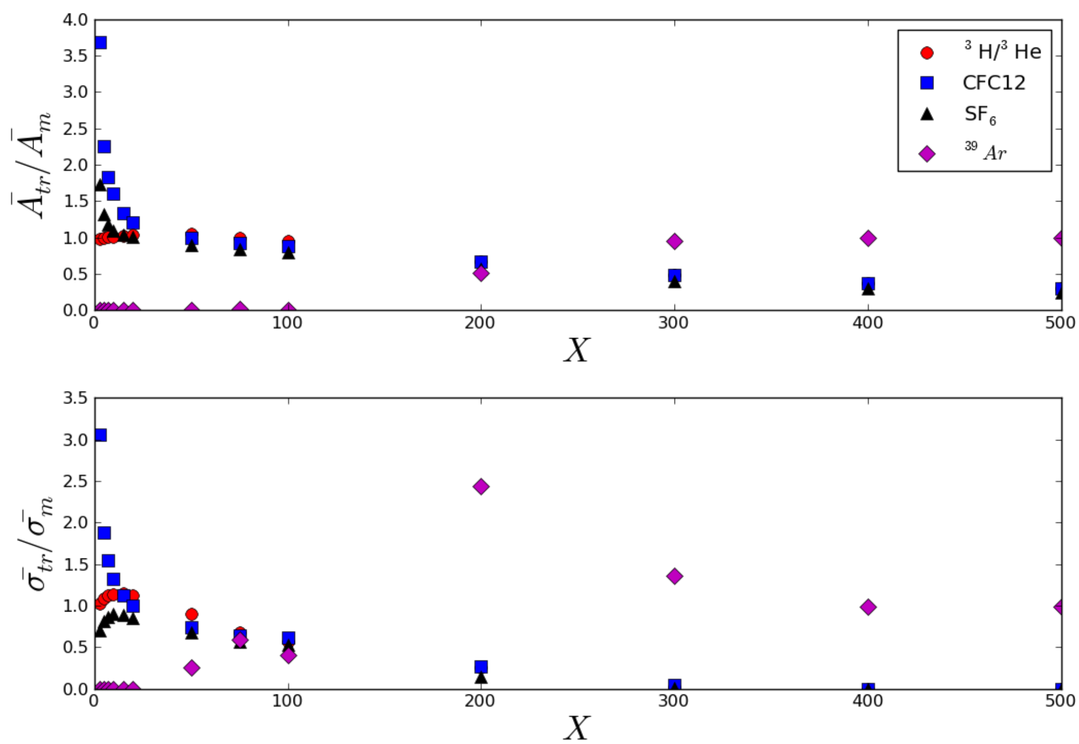

Figure 6 - Average tracer-derived age ($\bar{A}_{tr}$ - top) and standard deviation ($\bar{\sigma}_{tr}$ - bottom) for age distributions in y-z planes at increasing flow path length (*X*) normalized by average ($\bar{A}_m$) and standard deviation ($\bar{\sigma}_m$) of the modeled mean age distribution for a 3-D field. Triangles, squares, circles and diamonds are the moments derived from SF_6, CFC-12, ^{3}H/^{3}He and ^{39}Ar concentrations respectively.

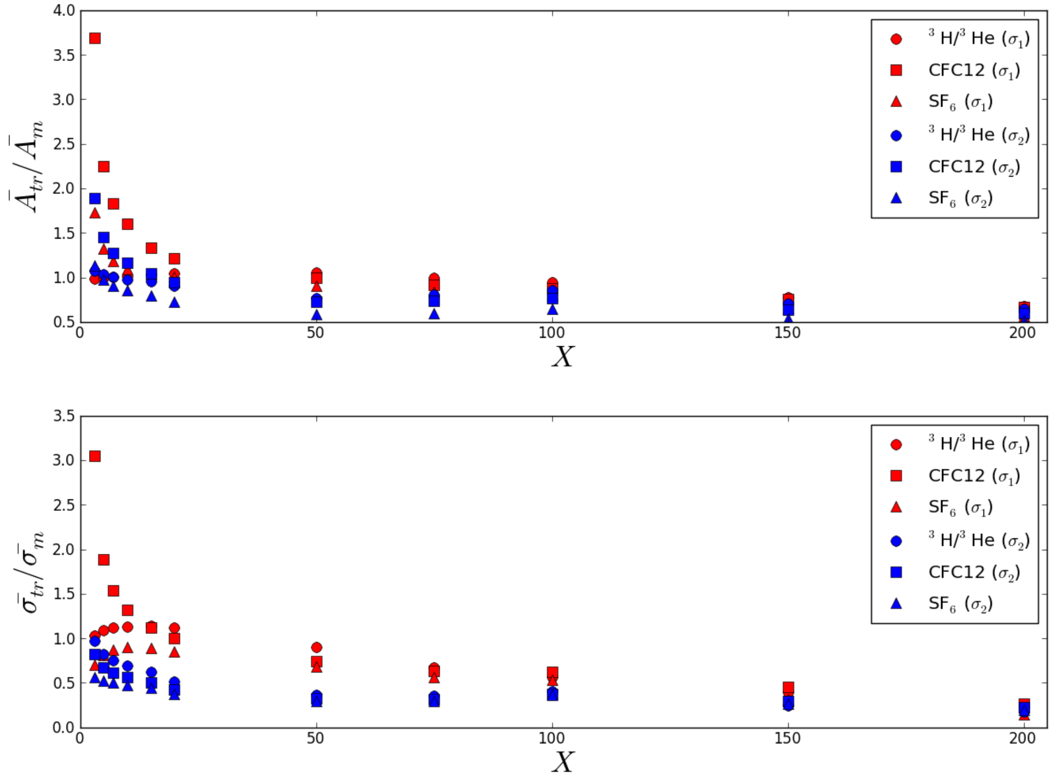

Figure 7 - Average tracer-derived apparent age ($\bar{A}_{tr}$) and standard deviation ($\bar{\sigma}_{tr}$) for age distributions in *y-z* planes normalized by average modeled mean age ($\bar{A}_m$) and standard deviation of the modeled mean age ($\bar{\sigma}_m$) distribution as flow path distance increases for the 3-D case. Values plotted for lognormal heterogeneous permeability fields with one (σ_1) and two (σ_2) orders of magnitude log normal standard deviations.

Using this computational platform we can explore the difference in 2-D and 3-D age distributions given the same spatial heterogeneity statistics. We start by comparing average modeled mean age in the y-z plane at a given flow path distances. The modeled mean age is less for 3-D ($\bar{A}_{3D}$) domains than for the 2-D ($\bar{A}_{2D}$) case, consistent with Pohll et al. 2000) (Figure 8). The difference between 2-D and 3-D age has maximum value of 1.4 (close to 40 percent higher) early in the flow path, falls to a minimum of around 1.2 near 1 correlation length (20 m) and then reaches an approximately constant value of 1.3 for flow distances over 20 m. The 2-D average age is still overestimated even when the flow path is over 25 times the correlation length. The overestimation of 2-D age is observed in the tracer-derived age using $^3H/^3He$ concentrations early in the flow path; however, the difference between 2-D and 3-D age diminishes at flow paths greater than 300 m as the age limit of the tracer is encountered.

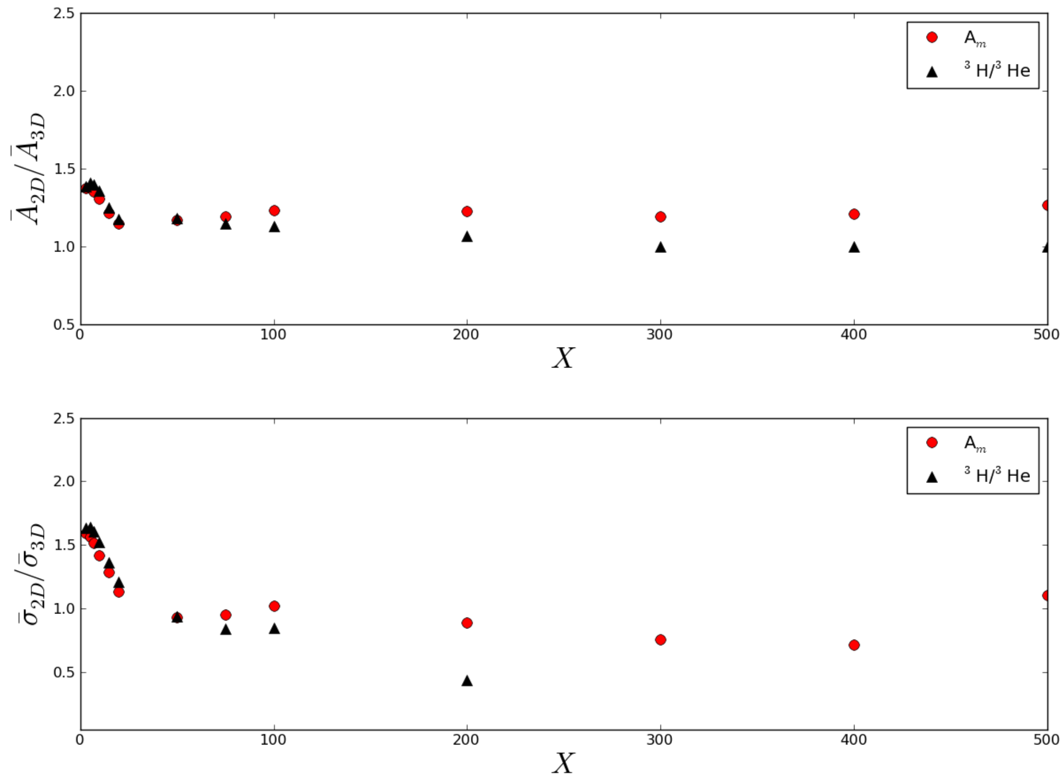

Figure 8 - 2-D average modeled age ($\bar{A}$ - top) and standard deviation ($\bar{\sigma}$ – bottom) normalized by the 3-D value for y-z planes at x distance (X). 2-D and 3-D heterogeneous fields have identical spatial correlation lengths with 1 order of magnitude lognormal standard deviation in the permeability field.

The spatial variance in modeled mean age is overestimated early in the flow path in the 2-D ($\bar{\sigma}_{2D}$) domain with a maximum value of 1.5 (Figure 8). The difference in spatial variance between the 2-D and 3-D case is close to zero (ratio of 1.0) for flow paths between 20 and 200 m (2-10 times the correlation length). At 500 m the difference in modeled age between 2-D and 3-D is higher. Similarly, the variance in age derived from the ^{3}H/^{3}He distribution is higher in the 2-D case compared to the 3-D. However, since the age limit is encountered at shorter flow distances in the 2-D case due to the longer travel times, the spatial variance in the 2-D case goes to zero and variance in the tracer-derived age distribution will actually be less than in the 3-D case.

The overestimation of age considering 2-D transport increases when the degree of heterogeneity is increased (Figure 8 and Figure 9). The maximum 2-D overestimation in $\bar{A}_m$ is about 40% for 1 order of magnitude lognormal standard deviation versus 100% for 2 orders of magnitude. The overestimation of variance in age distribution in the 2-D case is also increased for more heterogeneous permeability fields.

By modeling the full spatial distribution of mean age, the amount of age homogenization can be investigated. Even with a very modest amount of heterogeneity in the permeability field (i.e. one order of magnitude standard deviation), homogenization of age does not occur even after flow path lengths greater than 25 correlation lengths. Significant age heterogeneity is the rule rather than the exception. The amount of spatial variance in age was underestimated by tracer-derived ages. It is important to recognize, that significant variance in age is to be expected even in homogenous aquifers, and that even if a reasonable distribution of tracer samples is available, the true variation in age will be greater than that indicated by the tracers.

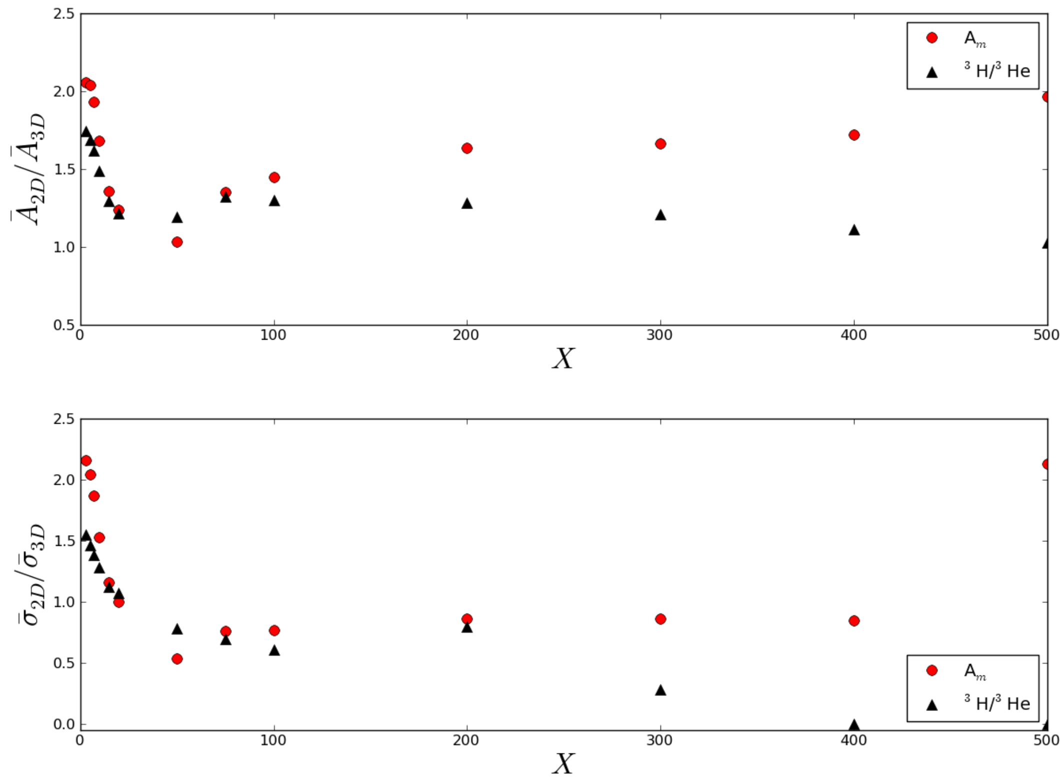

Figure 9 - 2-D average modeled age ($\bar{A}$ - top) and standard deviation ($\bar{\sigma}$ – bottom) normalized by the 3-D value for y-z planes at x distance (X). 2-D and 3-D heterogeneous fields have identical spatial correlation lengths with 2 orders of magnitude lognormal standard deviation in the permeability field.

2.3 Discussion

Our results show systematic bias toward younger ages in the spatial distribution of tracer-derived ages due to the effect of age limits. These findings are analogous to those reported by Larocque et al. (2009), McCallum et al. (2013), Weissman et al (2002), and Varni & Carrerra (1998) for the age distribution at a single point. It is clear in many cases that the modeled mean age can deviate significantly from the tracer-derived mean age even in relatively homogenous systems. Thus, calibration of groundwater models by matching modeled mean age to a tracer-derived apparent age will problematic in most systems. A better methodology would be to calibrate flow and transport models to tracer concentration as suggested by Bethke & Johnson (2008). High performance codes such as PFLOTRAN provide the necessary computational power to perform simulations with multiple environmental tracer concentrations for calibration.

We show that the degree of underestimation in average age and age variance increases with increasing levels of heterogeneity, which compares well with the results of McCallum et al. (2013). Our work adds further insight to this behavior by investigating the effect of considering only 2-D flow. The addition of the 3rd dimension increases flow path connectivity, decreasing the mean age at a given flow path distance, thus reducing the age bias for a given level of heterogeneity. The addition of flow in the 3rd dimension reduces spatial variance in age distribution; as a result the spatial variance in modeled age is generally overestimated when only 2-D flow is considered. For the simple case where correlation lengths are considered equal in all directions, the relative effect of increasing heterogeneity on age bias will be less in 3-D flow systems. However, considerable work on the role of the heterogeneity structure in 3-D systems remains to be done.

2.4 Conclusion:

In this paper, we use a massively parallel flow and transport code to simulate the concentrations of many environmental tracers with age information over a large range in time scales. We show that simulation of many tracer species in high-resolution, three-dimensional heterogeneous domains is possible. We report on simulations with meshes over 10 million nodes, and simulation time periods over 100,000 years, which can be run with wall clock times less than two hours when spread over 800 processors. The highly linear scaling performance of PFLOTRAN implies that even larger meshes can be run within reasonable times by advancing to larger computational platforms. At present the only limitation is the restriction to 32-bit integers in the third-party software HDF5 as implemented for Fortran90 to roughly two billion degrees of freedom. This capability allows for the investigation of tracer concentration distributions and derived "apparent" ages at unprecedented resolution with a much more complete set of physics. Simulated random permeability fields were used to explore tracer transport through heterogeneous 2-D and 3-D fields for many different tracers. Significant heterogeneity exists in the spatial distribution of mean age even in relatively homogenous domains after flow path lengths 25 times the spatial correlation length. Tracer-derived ages show systematic biases toward younger ages when the groundwater age distribution contains water older than the maximum tracer age. This bias toward younger ages increases for more heterogeneous systems; however, the effect of heterogeneity is diminished as the mean travel time gets closer the tracer age limit. The addition of the third dimension increases connectivity by adding another degree of freedom for groundwater flow. Mean age and spatial variance in age is decreased in 3-D systems relative to 2-D systems. Similar tracer-derived age bias effects are observed in 3-D systems; however, the magnitude of bias is reduced for a given flow path length and level of heterogeneity. High performance computational tools offer the computational power to explore the effect of heterogeneity on the age distribution in complex, high-resolution 3-D domains, offering groundwater hydrologists the ability to better understand tracer data in real world settings.

3. EVALUATION OF PARAMETER UNCERTAINTY REDUCTION IN GROUNDWATER FLOW MODELING USING MULTIPLE ENVIRONMENTAL TRACERS

3.1 Introduction

Calibration of groundwater flow models for the purpose of evaluating flow and aquifer heterogeneity typically uses observations of hydraulic head in wells and appropriate boundary conditions. However, groundwater models are often under constrained by hydrologic data alone, leading to significant uncertainty in model parameters and predictions, particularly regarding contaminant transport within the groundwater flow system. Joint calibration with solute transport information further constrains models and can significantly reduce the uncertainty in parameter estimates from the calibration process. Groundwater environmental tracers have a wide variety of decay rates and input signals in recharge, resulting in a potentially broad source of information to further constrain flow rates and parameter heterogeneity.

Environmental tracer data are frequently utilized in groundwater studies by calculating groundwater ages at different locations in the flow system and comparing the inferred ages to predictions based on physical groundwater hydrology principles and models. There are several drawbacks and limitations to this approach. The concept of a single groundwater age for a water sample implicitly assumes one-dimensional plug flow through the groundwater flow system, without consideration of mixing, dispersion, or diffusive mass transfer of tracer mass between mobile and immobile zones. Such mixing processes can lead to significant bias in the average groundwater age calculated for a groundwater sample and to discordant groundwater ages from different environmental tracers [Weismann et al., 2002; McCallum et al., 2013]. Thus, the use of groundwater "age" as a calibration data set [e.g., Portniaguine and Solomon, 1998; Sanford et al., 2004; Sanford, 2011], where modeled mean groundwater age is compared to tracer derived mean ages for groundwater samples, requires significant assumptions about the age distribution of a given sample.

Alternatively, environmental tracer data can be used by directly comparing the measured and simulated concentrations from a groundwater flow and solute transport model during the groundwater model calibration process. This approach has the advantage of bypassing the assumptions inherent in the groundwater age approach and provides a means of directly integrating transport and velocity information from environmental tracers into calibration constrained uncertainty analyses of groundwater flow and solute transport. However, this approach does depend on numerical simulations of flow and solute transport of sufficient resolution and accuracy to capture the effects of mixing processes, such as dispersion and diffusion.

The objective of this study is to evaluate the reduction of uncertainty in groundwater flow model parameters using environmental tracer concentrations for multiple tracers, in combination with hydraulic data in the direct simulation approach described above. This evaluation is conducted using a model of a two-dimensional, synthetic aquifer with heterogeneous permeability and porosity. Steady-state groundwater flow and transient tracer transport are simulated using the PFLOTRAN software code [Hammond et al., 2012], resulting in the synthetic reality from which data at well locations are extracted. These data on pressures and tracer concentrations are then used as observations for automated calibration of a simplified flow and transport model using the pilot point method and the PEST code [Doherty, 2009]. Optimization runs are performed to estimate parameter values of permeability and linear confidence intervals at the 30 pilot points in the model domain.

3.2 Background

Environmental tracers have traditionally been used to assess the apparent age of groundwater samples. However, groundwater samples are not composed of water of a single age but an age distribution and the environmental tracer concentration at the sampling point is a function of the age distribution and the tracer concentration history described by the convolution integral. Lumped parameter models can be used to calculate the flux averaged mean age of groundwater samples by assuming an age distribution within the groundwater system. Different groundwater age distributions will lead to different mean ages for a given tracer concentration [e.g., Corcho Alvarado et al., 2007; Gardner et al., 2011; Solomon et al., 2010]. The use of multiple tracers can help reduce the uncertainty in the most applicable age distribution [Corcho Alvarado et al., 2007; Gardner et al., 2011; Solomon et al., 2010].

Groundwater mean age can be modeled using the advection dispersion equation [Goode, 1996]. The information contained in the groundwater age distribution has been shown to be useful in constraining groundwater models [Murphy et al., 2011; Portniaguine and Solomon, 1998; Sanford, 2011; Sanford et al., 2004; Troldborg et al. 2008]. Most commonly mean groundwater age is modeled, and compared to the apparent mean age determined by a single tracer concentration assuming a piston flow age [e.g., Portniaguine and Solomon, 1998; Sanford, 2011; Sanford et al., 2004]. The calculation of apparent mean age of a groundwater sample from a tracer concentration requires a significant assumption about the age distribution in the groundwater sample. Corcho Alvarado et al. [2007] use multiple tracer concentrations and a combined lumped-parameter, advection-diffusion approach to attempt to calculate the age distribution which best matches the combined tracer concentrations; however, the ability to determine the best age distribution model is still subjective.

In many cases the tracer-derived mean age will not be equal to the true groundwater mean age. Weissmann et al. [2002] simulate the age distribution and show that the CFC determined mean age is not equal to the water mean age due to the truncation of age information on waters over 70 years for young tracers. More recently, McCallum et al. [2013] show that this age bias is a function of the degree of heterogeneity in the system and bias will increase for higher degrees of heterogeneity.

Bethke and Johnson [2008] argue that given the complexity of interpreting groundwater mean age and/or age distribution from tracers, a better approach is to simulate concentrations of tracers and calibrate models to tracer concentrations. Tracer concentration distribution can provide significant constraint on conceptual and numerical models of groundwater flow and transport. For example, Bethke et al. [1999] and Zhao et al. [1998] show that helium isotopic distribution can be used in conjunction with a numerical model to understand a regional scale flow system. Castro et al. [1998] use multiple noble gas tracers to help calibrate a 2-D flow and transport model of the Paris Basin. The addition of noble gases was beneficial in constraining the permeability of the reservoir system. Troldborg et al. [2008] simulate the age distribution at a point using particle tracking and calculate the expected CFC concentration using the convolution integral and then calibrate to the CFC concentration. Recently Gardner et al. [2013] use a massively parallel flow and transport code to simulate multiple environmental tracer concentrations in high resolution 2-D and 3-D domains, showing that the direct simulation of multiple tracer concentrations can be achieved with modern parallel computational platforms.

In all cases tracer concentrations have been shown to be beneficial in calibration of groundwater flow and transport models. Here we formally calculate the reduction in parameter uncertainty using direct simulation of multiple environmental tracer concentrations in a synthetic aquifer. Groundwater flow modeling constitutes a synthesis of available data, a numerical representation of the conceptual model of the physical system, and a predictive tool for potential future configurations of the groundwater flow system. Model calibration is achieved by adjusting model parameters to minimize the difference between observations of the system and simulated state variables. Originally obtained by trial-and-error adjustments to model parameters, optimization of the groundwater flow model calibration is now typically achieved with automated methods that systematically seek to minimize the calibration error.

Differing model parameterization strategies may use a minimal number of parameters to preserve parsimony [e.g., Hill and Tiedeman, 2007] or advocate the use of highly parameterized models [e.g., Doherty et al., 2010 and Hunt et al., 2007] to allow full utilization of information about the system and more fully explore the range of model uncertainties. Given the inherent lack of knowledge about complex subsurface groundwater systems, a primary objective of groundwater flow modeling should be an evaluation of uncertainty in model parameters and model predictions.

Groundwater models are often nonunique, in the sense that various combinations of parameter values result in model outcomes that match observations nearly equally well. Predictive analysis calculates the effects of this parameter uncertainty, as estimated through the calibration process, on model predictive uncertainty. Various methods, including linear and non-linear methods, can be employed in the evaluation of model uncertainty. Linear uncertainty quantification is accomplished by evaluating the sensitivity of the model to input parameters in the region of the solution space near the optimal calibration. Metrics of linear parameter uncertainty include confidence intervals based on an assumed Gaussian uncertainty distribution [Hill and Tiedeman, 2007; Doherty, 2009], and parameter identifiability [Doherty and Hunt, 2009]. Numerous methods are available for calibration constrained nonlinear uncertainty analysis, including nonlinear prediction intervals [Vecchia and Cooley, 1987; Christensen and Cooley, 1999], and null space Monte Carlo [Tonkin et al., 2007]. Although linear uncertainty analysis may be inaccurate relative to nonlinear analytical methods, linear uncertainty analysis is used in this study because the flow and transport model is relatively well constrained by synthetic observational data and the objective is to determine the relative uncertainty reduction among the observational data sets.

3.3 Model Setup

The evaluation of uncertainty in groundwater flow model parameters consists of the following steps: (1) development of the conceptual model and construction of a synthetic aquifer, (2) simulation of groundwater flow and environmental tracer transport, (3) extraction of synthetic observational data from the simulation results, and (4) automated calibration of a simplified flow and transport model using the synthetic observational data as calibration targets. Use of a representative synthetic aquifer and high resolution flow and transport model provides access to the “true” characteristics of the groundwater flow system and *in situ* tracer concentrations. The simplified flow and transport model is typical of the simulation capabilities for a fairly well characterized, but incompletely known, groundwater flow and transport system. Uncertainty in the permeability values used in the simplified groundwater model is determined from the model sensitivities calculated during the automated calibration, or optimization, of the model.

The synthetic aquifer and groundwater model used in this study consists of a two-dimensional domain that is 500 m by 500 m. The conceptual model of the groundwater flow system represented in this model is a heterogeneous, anisotropic, confined aquifer consisting of a porous medium with steady-state groundwater flow, as shown in Figure 10. Groundwater flow boundary conditions to the system are specified pressure on the west and the east sides (corresponding to an average head gradient of about 0.01 m/m), and no flow on the upper, lower, north and south boundaries. Environmental tracer concentrations are specified in the recharge at the western boundary of the model, based on historical records of atmospheric concentrations, as indicated in Table 3 (Appendix A:). Average annual tracer concentrations in the aqueous phase were calculated from atmospheric concentration data and assuming a recharge temperature of 25ºC. Pre-modern initial conditions for ^3H, ^3He, and ^{39}Ar are at steady state in the flow system and input of anthropogenic CFC11 and ^3H concentrations in recharge vary with time beginning in 1940. The tracers ^3H, and ^{39}Ar are subject to radioactive decay, with half lives of 12.3 years and 269 years, respectively. Tritium decays to ^3He within the flow system. Ingrowth of ^3He from mineral grains in the aquifer is neglected, given the relatively short time- and length-scales of the flow and transport system. All tracers were assumed to be non-sorbing and chemically inert, which is reasonable for these tracers [Cook and Herczeg, 2000].

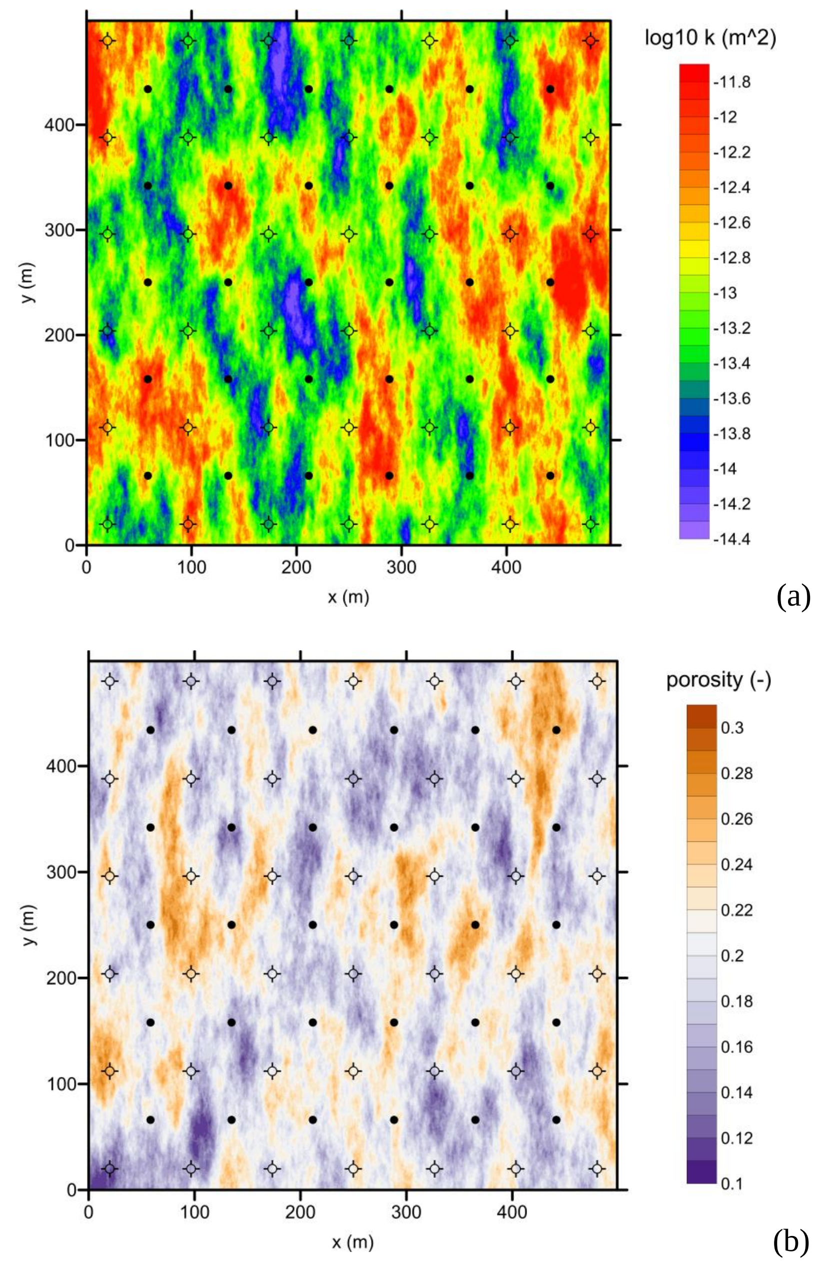

Figure 10 - Heterogeneous permeability field (a) and porosity field (b) in the synthetic aquifer model. Open crossed circle symbols are observation points and filled circles are pilot points.

Geostatistical simulation is used to create the heterogeneous permeability and porosity fields in the synthetic aquifer of the groundwater model, as shown in Figure 10. Random, unconditional sequential Gaussian simulation method [Deutsch and Journel, 1998] is used with a lognormal distribution of permeability and normal distribution of porosity. The geometric mean of the permeability values in the sequential Gaussian simulation is 1×10^{-13} m^2 and the standard deviation is one order of magnitude. The distribution of porosity has a mean value of 0.20 and a standard deviation of 0.03. Values of permeability and porosity are uncorrelated in the synthetic

aquifer. Anisotropic spatial correlation is specified in the sequential Gaussian simulation, with a correlation length of 80 m in the *y* direction (north-south) and 40 m in the *x* direction (east-west). The model domain is large enough to encompass more than six correlation lengths in the *y* direction and more than 12 correlation lengths in the *x* direction. The anisotropic spatial correlation of permeability and porosity is evident in the color-scale plots shown in Figure 10. Note that the flow boundary conditions result in average groundwater flow perpendicular to the major axis of spatial correlation in permeability. Although this choice of relative orientation between the hydraulic gradient and heterogeneity is arbitrary, it corresponds to the hydrogeologically realistic situation at the margin of a sedimentary basin in which groundwater flow is down dip through shoreline facies oriented parallel to strike of the aquifer.
The groundwater flow and transport model for the synthetic flow system is implemented with the PFLOTRAN software code. The governing equations and numerical methods utilized in PFLOTRAN are described in Hammond et al. [2012]. PFLOTRAN is a scalable, parallel, multi-phase, multi-component, non-isothermal reactive flow and solute transport code using a fully implicit, integral finite volume formulation. The grid for the groundwater flow and transport model is an orthogonal mesh with a cell spacing of 1 m. A very long flow and transport simulation is performed to establish the steady-state distribution of pressure and tracer concentrations for the pre-modern tracers, which is then used as the initial conditions for a simulation from 1940 to 2012 that includes the time-varying recharge concentrations for the anthropogenic tracers.

Simulated results from the synthetic groundwater flow and transport system model for 2012 are shown in Figure 11 and Figure 12. A contour plot of simulated pressure is shown in Figure 11(a). Comparison of Figure 11(a) to Figure 10(a) reveals the correspondence of areas with higher hydraulic gradient to areas of lower permeability and of areas with lower hydraulic gradient to areas of higher permeability, as expected. Considerable variations in simulated ^{39}Ar concentration and the high spatial resolution of these variations in Figure 11(b) indicate transport times of up to several hundred years through the system and the high sensitivity of ^{39}Ar concentration to heterogeneity in the synthetic aquifer. Simulated CFC11 concentrations shown in Figure 12(a) indicate limited variability in concentration with the CFC11 front in the simulated aquifer somewhat smeared by dispersion. The absence of CFC11 over most of the model domain shows that only limited information on the groundwater flow system and heterogeneity is provided by the CFC11 data. Simulated ^{3}H concentrations in Figure 12(b) show somewhat more variability than CFC11, due to greater variation in the ^{3}H concentration in recharge and radioactive decay during transport. The pattern of ^{3}H concentrations in Figure 12(b) suggests lower information content regarding aquifer heterogeneity in these data than for ^{39}Ar.

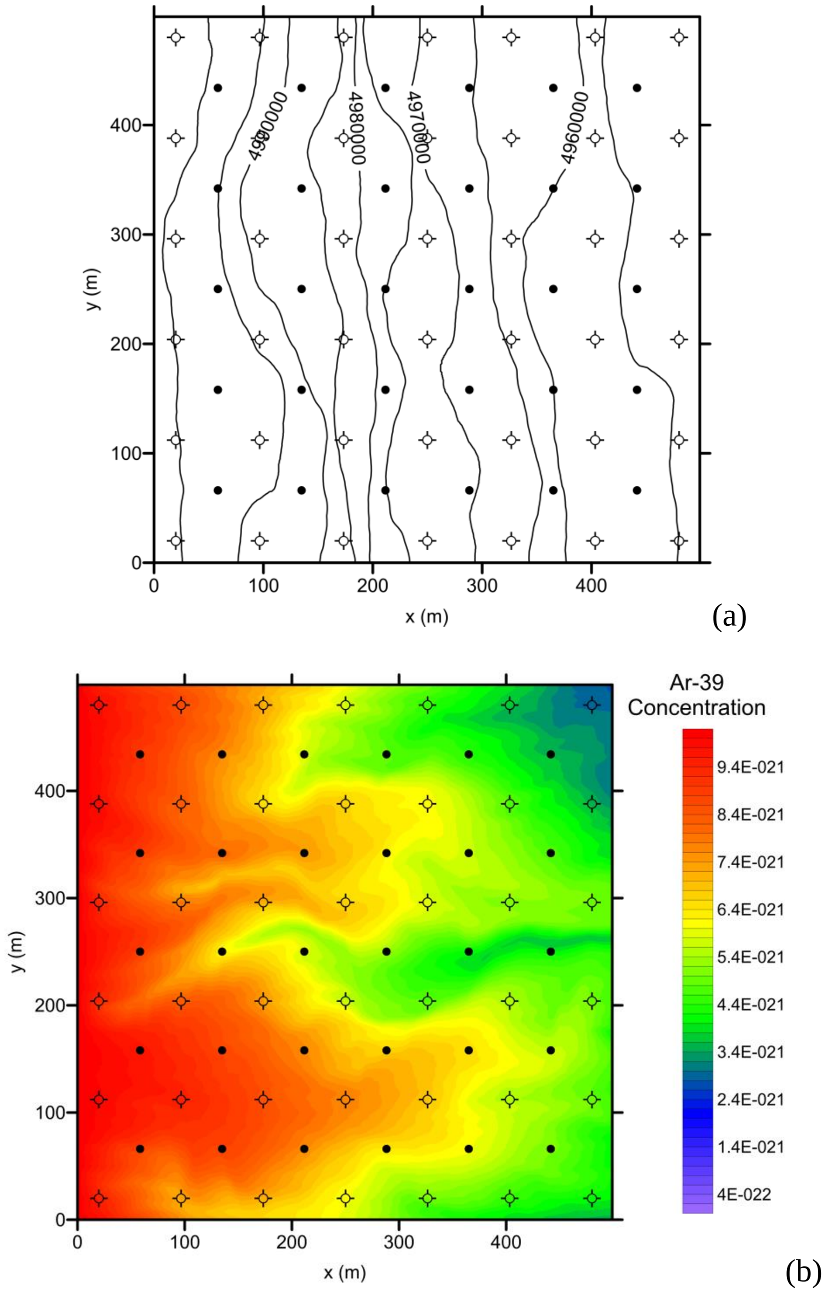

Figure 11 - Simulated pressure contours (Pa) (a) and ^{39}Ar concentration (mol/kg) in the synthetic aquifer model (b). Open crossed circle symbols are observation points and filled circles are pilot points.

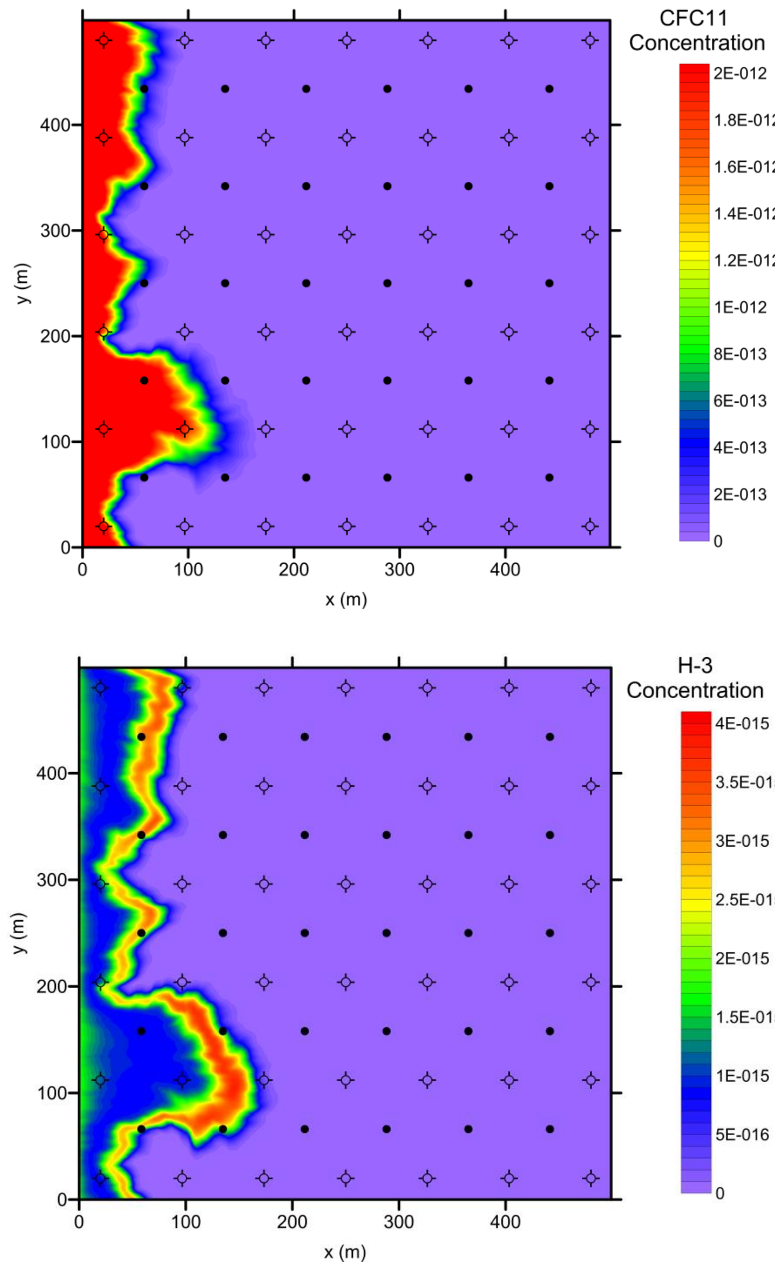

(a)

(b)

Figure 12 - Simulated CFC11 concentration (mol/kg) (a) and ^3H concentration (mol/kg) in the synthetic aquifer model (b). Open crossed circle symbols are observation points and filled circles are pilot points.

Observations of pressure and environmental tracer concentrations at the end of the simulation time, corresponding to the year 2012, are extracted from the synthetic groundwater system model at 42 locations, corresponding to hypothetical wells in the aquifer. The 42 locations are defined by a regular grid of sites shown with the open crossed circle symbols in Figure 10. These synthetic observational data are used as calibration targets in the simplified flow and transport model and are tabulated in Table 4 in the Auxiliary Material. Various subsets of these observation data are used in the different calibration and uncertainty analysis cases described below.

The simplified groundwater flow and transport model embodies the same conceptual model of the groundwater system described for the synthetic groundwater model, but lacking the detailed knowledge of aquifer heterogeneity in permeability and porosity. The simplified groundwater model represents the kind of model that would be constructed by an investigator who has general knowledge of the geology, dimensions, and boundary conditions of the groundwater system, but data on aquifer properties, pressure, and environmental tracer concentrations at a limited number of observation wells.

The simplified groundwater flow and transport model is calibrated using automated methods with the PEST software code [Doherty, 2009]. PEST is a model-independent set of computer codes for model inversion, parameter estimation, and uncertainty analysis. PEST was linked to the simplified groundwater flow and transport model in this study to find the optimal calibrated set of parameter values, based on the synthetic observational data, and to evaluate the linear uncertainty in those parameter values. The nonlinear Levenberg-Marquardt algorithm is an iterative method used in PEST to solve the inverse problem for the associated model. This is a computationally efficient gradient-based inversion method that uses the derivative sensitivity of the observations with respect to the parameters to determine the optimal values for the input parameters.

The pilot point method is often used for the parameterization of heterogeneous fields in groundwater flow model calibration [RamaRao et al., 1995; Doherty, 2003; Doherty et al., 2010]. In this approach, parameter values are assigned at pilot point locations and values are interpolated at other locations based on a measured or assumed spatial correlation structure [de Marsily et al., 1984]. The 30 pilot point locations used in the calibration of the simplified flow and transport model are shown as the filled circles in Figure 10. The values of permeability at the pilot points are adjusted in the calibration process to obtain an optimal match between observed and simulated pressure and tracer concentrations. The values of permeability at other locations in the model domain are calculated using the kriging interpolation method [Deutsch and Journel, 1998] and a spatial correlation structure approximately equal to the underlying synthetic aquifer properties. Information on the correlation length and the anisotropy of permeability and porosity in the aquifer is conceptually available from measurements at the 42 hypothetical wells in the synthetic aquifer.

Calibration of the simplified groundwater flow and transport model is achieved by minimizing the objective function that is defined by the sum of weighted, squared differences between observed and simulated values of pressure and tracer concentrations. Weighting values for different types of observations (i.e., pressures and different tracer concentrations) are assigned to approximately equalize the contributions of the different observation types to the objective function, thereby assuring equal utilization of information from different data sources. Input parameter values for permeability are log transformed in the calibration process and porosity is untransformed. Values of permeability at the 30 pilot points are treated as adjustable parameters and values of porosity are fixed at the average value of 0.20. Although spatial variability in porosity exists in the synthetic aquifer, its impact on tracer concentrations is significantly less than the impact from heterogeneity in permeability. Additional uncertainty in the model calibration would be introduced by considering variability in porosity; however, that uncertainty was not investigated in this study.

3.4 Results

Four cases are analyzed by calibration of the simplified groundwater flow and transport model using various combinations of observational data with the PEST code: (1) pressure data only, (2) pressure and CFC11 concentrations, (3) pressure and ^{39}Ar concentrations, and (4) pressure, CFC11, ^{39}Ar, ^{3}H, and ^{3}He concentrations. The automated calibration process successfully achieves minimization of the objective function for all four cases using reasonable ranges of values for permeability at the 30 pilot points.

The match between observed synthetic measurements and simulated values for Case 3 (pressure data and ^{39}Ar concentrations) is shown graphically in plots of simulated versus observed values in Figure 13. The plot of simulated versus observed values of pressure in Figure 13(a) shows a very good calibration of the simplified groundwater flow and transport model with regard to pressure, as indicated by the clustering of the 42 points along the dashed red line, which corresponds to a perfect match between simulated and observed values. The plot of simulated versus observed ^{39}Ar concentrations in Figure 13(b) shows a poorer match than for the pressure data, in relative terms. This difference in the calibration results for pressure and ^{39}Ar concentrations is consistent with the fact that fluid pressure is a much more diffusive property of the system than solute concentration. Values of pressure at an observation point tend to average the effects of permeability heterogeneity over a relatively large volume of the aquifer, whereas tracer concentration at a given location is sensitive to heterogeneity at a much smaller spatial scale. The larger error in ^{39}Ar concentrations compared to pressure illustrates the limitation in pressure alone being able to distinguish the difference between the simplified and true model, while it is apparent that the simplified model cannot completely explain the tracer concentration fields. The error residuals for both pressure and ^{39}Ar concentration are approximately normally distributed with mean values of about zero, indicating that the calibration results are unbiased. Figure 14 shows the kriged permeability field and the simulated ^{39}Ar concentrations in the calibrated simplified groundwater flow and transport model for Case 3 (pressure data and ^{39}Ar concentrations). The kriged permeability field in Figure 14(a) illustrates the degree of simplification inherent in the pilot point approach to modeling aquifer heterogeneity, in comparison to the “true” nature of the heterogeneity in the synthetic aquifer shown in Figure 10(a). Nonetheless, the kriged permeability field in the simplified flow and transport model matches some of the gross features of the synthetic aquifer and provides a close match to the pressure data (Figure 13(a)). The simulated ^{39}Ar concentrations in the calibrated model shown in Figure 14(b) also matches the gross features of the spatial variability in the simulated ^{39}Ar concentrations from the synthetic aquifer model (Figure 11(b)), and correspond to an adequate match between simulated and observed values (Figure 13(b)).

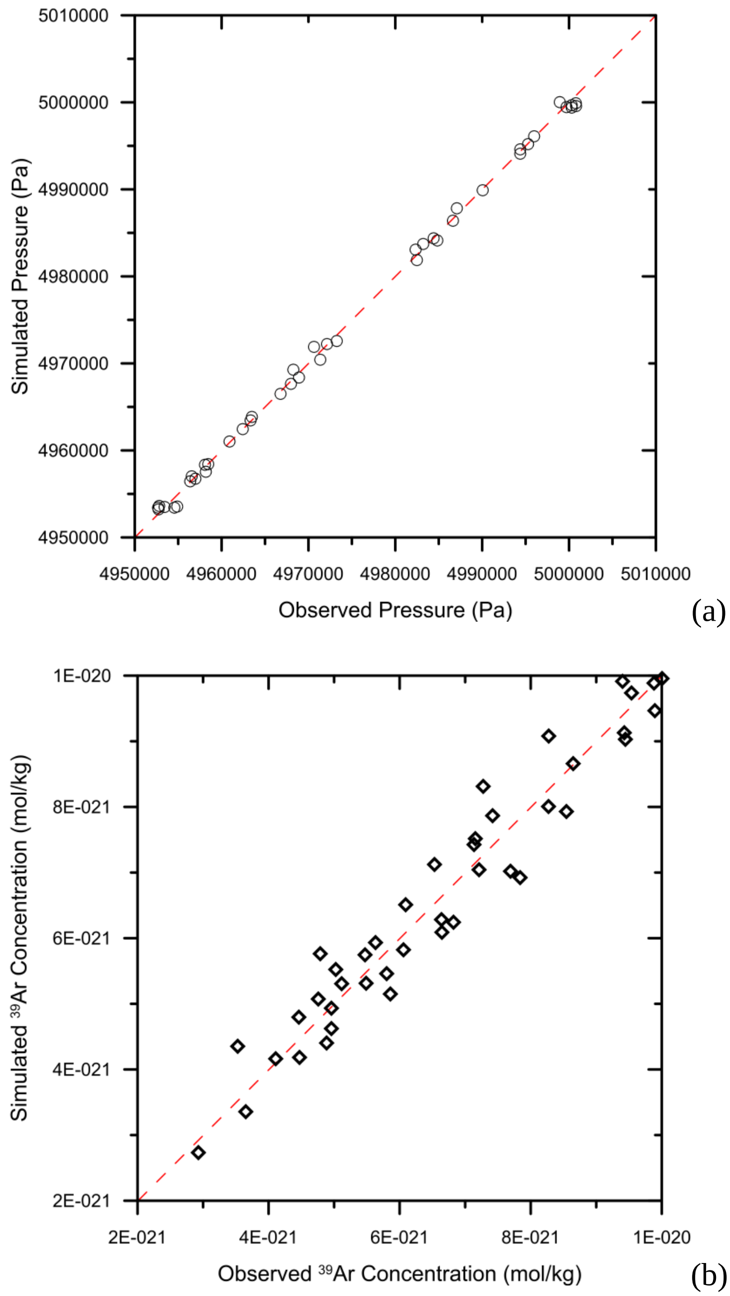

Figure 13 - Simulated versus observed pressure (a) and ^{39}Ar concentration (b) from the groundwater flow and transport model calibrated with observations of pressure and ^{39}Ar concentration.

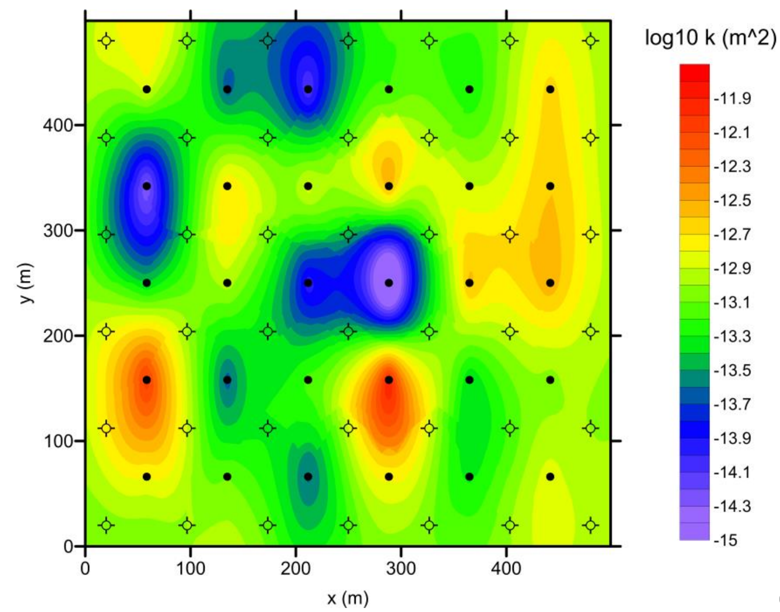

(a)

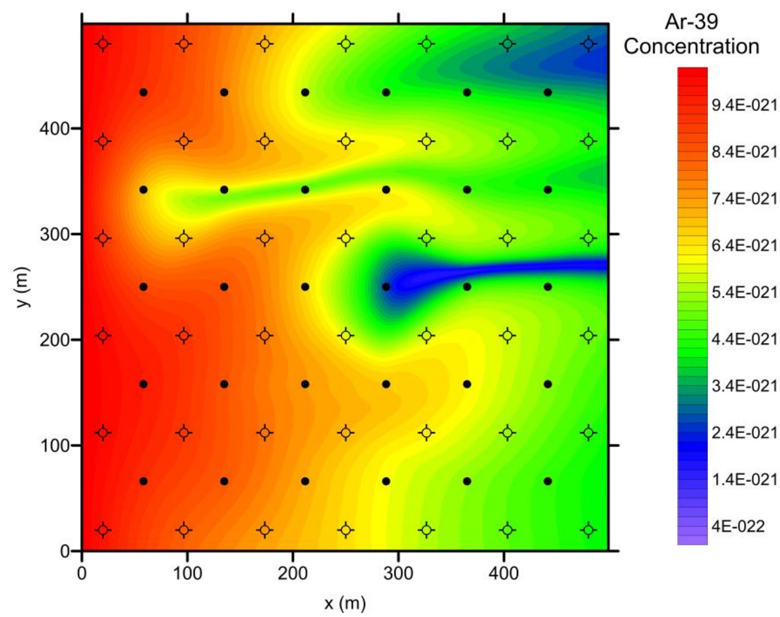

(b)

Figure 14 - Kriged permeability field from the calibrated flow and transport model (a) and simulated ^{39}Ar concentration (mol/kg) (b) from the calibrated flow and transport model using observations of pressure and ^{39}Ar concentrations. Open crossed circle symbols are observation points and filled circles are pilot points.

Uncertainty in the estimated values of permeability at the 30 pilot points from the calibrated simplified groundwater flow and transport model is evaluated using the linear 95% confidence intervals from the PEST code. Linear uncertainty is calculated from the parameter sensitivities in the Jacobian matrix in the solution space near the optimized model parameters assuming a Gaussian error distribution. Figure 15 shows plots of the calibrated values of permeability at the 30 pilot points and the 95% confidence intervals for the four cases of observational data considered in this study. Note that the *y* axis in the plots in Figure 15 is $\log_{10}$-transformed permeability, so ranges of uncertainty in permeability span several orders of magnitude in some instances. Visual examination of Figure 15(a) to Figure 15(d) indicates that the ranges of uncertainty in values of permeability at the pilot points are significantly lower for cases that include observational data on environmental tracer concentrations relative to Case 1 in which data on pressure alone are used. Inspection of the plots also shows that the ranges of uncertainty are lower for Cases 3 and 4 that include ^{39}Ar concentration data in comparison to Case 2, which includes tracer concentration data of CFC11 alone.

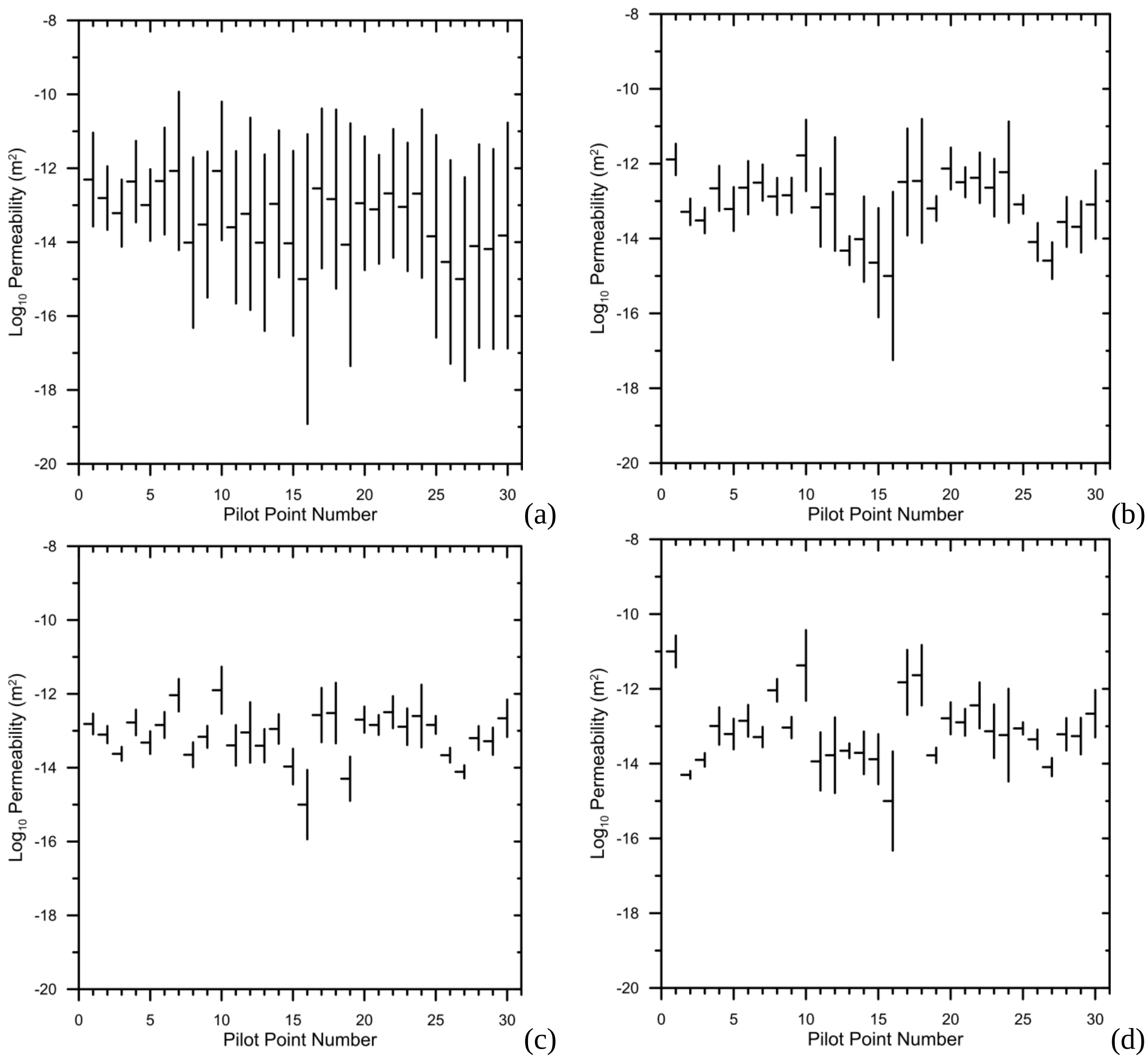

Figure 15 - Calibrated values (tic mark on left side of bars) and linear 95% confidence intervals (vertical bars) for permeability at the 30 pilot points in the flow and transport model calibrated with: (a) observations of pressure only, (b) observations of pressure and CFC11 concentration, (c) observations of pressure and ^{39}Ar concentration, and (d) observations of pressure, CFC11, ^{39}Ar, ^{3}H, and ^{3}He concentrations.

It should be noted that there are alternative metrics for uncertainty to the linear confidence intervals used in this evaluation. Uncertainty in model parameters and predictions can be highly non-linear, particularly for under-constrained models with highly correlated input parameters. Non-linear uncertainty can be estimated using a number of methods, as discussed in the Background section of this paper. However, the linear confidence intervals provide an adequate estimate of uncertainty for the purposes of this study, given the relatively well constrained nature of this synthetic flow and transport system model and the generally low correlation between input parameters reported by the calibration process.

Quantitative comparisons of uncertainty in permeability at the 30 pilot points and estimates of uncertainty reduction with the inclusion of additional tracer concentration data are shown in Table 2. By adding CFC11 observations to the calibration process, the average linear 95% confidence interval among the 30 pilot points is reduced from 4.6 orders of magnitude using only pressure data (Case 1) to 1.6 orders of magnitude (Case 2). The average 95% confidence interval is still lower at 0.9 orders of magnitude for Case 3 using pressure and ^{39}Ar concentration data, corresponding to an uncertainty reduction factor of 5.1 relative to Case 1. The uncertainty in permeability is slightly higher in Case 4 using combined tracer concentration data for CFC11, ^{39}Ar, ^{3}H, and ^{3}He relative to Case 3 using ^{39}Ar as the only source of data on tracer concentrations.

Table 2 - Model calibration results for optimization cases.

Case	**Observation Data**	**Average Linear 95% Confidence Interval Width - $\mathbf{Log_{10}}$ Permeability ($\mathbf{m^2}$)**	**Linear Uncertainty Reduction Factor Relative to Case 1**
1	pressure	4.6	1.0
2	pressure, CFC11 concentration	1.6	2.9
3	pressure, ^{39}Ar concentration	0.9	5.1
4	pressure,CFC11, ^{39}Ar, ^{3}H, ^{3}He concentrations	1.0	4.6

3.5 Discussion and Conclusions

Although the pilot point method constitutes a significant simplification of the spatial variability in permeability in the synthetic aquifer in this study, it provides a close calibration of the groundwater flow and transport model to pressure data and an adequate calibration to tracer concentration data. Lacking information on the detailed spatial structure of permeability and porosity in the subsurface, the pilot point approach is one of the most advanced methods of simulating aquifer heterogeneity and is appropriate for use in the evaluation of data worth and the uncertainty reduction from the use of environmental tracer data in groundwater modeling. However, the simplifications associated with the pilot point approach introduce structural errors to the simplified flow and transport model that result in irreducible uncertainty in parameter estimates and model predictions.

The direct use of environmental tracer data in groundwater model calibration results in a significant reduction in uncertainty in input parameter estimates for permeability relative to calibration based on hydraulic measurements alone. It is important to note that anthropogenic tracers and their decay products such as CFC11, ^{3}H, and ^{3}He provide significant constraint on input permeability values in the model, even when they have not been transported through much of the model domain, such as the case in this study (Figure 12). This is because these data provide information on the overall groundwater flux through the flow system, based on the transport distance of the tracer front. The relative sensitivities of the permeability values to the pressure observations effectively propagate the information on the anthropogenic tracers throughout the model domain to a certain extent, leading to a reduction in uncertainty in other parts of the model.

Tracer data for ^{39}Ar provide even more complete information on the heterogeneity of permeability and variability in the flow system than the anthropogenic tracers, leading to greater uncertainty reduction. Because ^{39}Ar is a decaying tracer with a continuous natural source and its half-life is well within the transport times of several hundred years in the synthetic aquifer it is well suited to provide information on the variability of groundwater flow and heterogeneity throughout the model domain. In other words, ^{39}Ar is well “tuned” to the characteristics of the groundwater flow system in this study regarding its ability to provide information on the system. One seemingly counterintuitive result of this study is that the average uncertainty in values of permeability is no lower and slightly higher when tracer concentration data for CFC11, ^{3}H, and ^{3}He are added to data on pressure and ^{39}Ar concentration in Case 4. This may be because these additional data sets contain largely redundant information on heterogeneity of the groundwater system. Such redundancy, combined with the structural error associated with the pilot point method discussed above may lead to a small broadening of the uncertainty in the input values of permeability. However, it should be noted, that without knowledge on the characteristic transport time of the aquifer, it would be impossible to know which tracer provides the best information, thus multi-tracer data sets are still recommended.

Overall, this study demonstrates the effectiveness of directly simulating environmental tracer concentrations in a high-resolution groundwater flow and transport model in the calibration process. With this approach the model directly matches the collected data, effectively bypassing potentially questionable assumptions associated with the calculation of groundwater age from tracer concentrations. In addition, the direct simulation of tracer concentrations provides a means of estimating the uncertainty in model input parameters and, potentially, in model predictions. This study also demonstrates that inclusion of environmental tracer data in the model calibration process can reduce the uncertainty in input values of permeability by orders of magnitude relative to calibration based on hydraulic head or pressure alone. An environmental tracer that is well “tuned” to the range of transport times through the groundwater flow system, such as ^{39}Ar in this case, provides the best information and maximum uncertainty reduction for model input parameters.

4. REFERENCES

Bethke, C.M. and T.M. Johnson (2008), Groundwater age and groundwater age dating, *Annual Review of Earth and Planetary Sciences*, ***36***, 121–152.

Bethke, C.M., X. Zhao, and T. Torgersen (1999), Groundwater flow and the ^{4}He distribution in the Great Artesian Basin of Australia, *J. Geophys. Res.*, ***104*** (B6), 12999–13011. http://dx.doi.org/10.1029/1999JB900085.

Castro, M.C., P. Goblet, E. Ledoux, S. Violette, and G. de Marsily (1998), Noble gases as natural tracers of water circulation in the Paris Basin: 2. Calibration of a groundwater flow model using noble gas isotope data, *Water Resour. Res.*, ***34*** (10), 2467–2483. http://dx.doi.org/10.1029/98WR01957.

Christensen, S. and R.L. Cooley (1999), Evaluation of prediction intervals for expressing uncertainties in groundwater flow model predictions, *Water Resour. Res.*, ***35*** (9), 2627–2639, *doi:*10.1029/1999WR900163.

Cook, P. and Herczeg, A.L., eds. (2000), *Environmental tracers in subsurface hydrology*, Kluwer Academic, Norwell, Massachusetts.

Corcho Alvarado, J. A., R. Purtschert, F. Barbecot, C. Chabault, J. Rueedi, V. Schneider, W. Aeschbach-Hertig, R. Kipfer, and H. H. Loosli (2007), Constraining the age distribution of highly mixed groundwater using 39Ar: A multiple environmental tracer (3H/3He, 85Kr, 39Ar, and 14C) study in the semiconfined Fontainebleau Sands Aquifer (France), Water Resour. Res., 43, W03427, doi:10.1029/2006WR005096.

Cornaton, F. & Perrochet, P. (2006a), 'Groundwater age, life expectancy and transit time distributions in advective-dispersive systems: 1. Generalized reservoir theory', Advances in Water Resources 29(9), 1267 – 1291.

Cornaton, F. & Perrochet, P. (2006b), 'Groundwater age, life expectancy and transit time distributions in advective-dispersive systems; 2. Reservoir theory for sub-drainage basins', Advances in Water Resources 29(9), 1292 – 1305.

de Marsily, G., G. Lavedan, M. Boucher, and G. Fasanino (1984), Interpretation of interference tests in a well field using geostatistical techniques to fit the permeability distribution in a reservoir model, in *Geostatistics for Natural Resources Characterization*, Part 2, pp. 831-849, D. Reidel.

Deutsch, C.V. and A.G. Journel (1998), *GSLIB – Geostatistical Software Library and User's Guide*, Oxford University Press, New York.

Doherty, J. (2003), Ground water model calibration using pilot points and regularization, *Ground Water*, ***41*** (2), 170-177.

Doherty, J.E. (2009), *Manual for PEST: Model Independent Parameter Estimation*, in: J.E. Doherty (Ed.). Watermark Numerical Computing, Brisbane, Australia, 336.

Doherty, J.E. and R.J. Hunt (2009), Two statistics for evaluating parameter identifiability and error reduction, *Journal of Hydrology**, 366*** (1-4): 119-127.

Doherty, J., M. N. Fienen, and R. J. Hunt (2010), *Approaches to Highly Parameterized Inversion: Pilot-Point Theory, Guidelines, and Research Directions*, U.S. Geol. Surv. Scientific Investigations Report 2010-5168, U.S. Geological Survey, Middleton, WI.

Gardner, W.P., D.D. Susong, D.K. Solomon, and H.P. Heasler (2011), A multitracer approach for characterizing interactions between shallow groundwater and the hydrothermal system in the Norris Geyser Basin area, Yellowstone National Park, *Geochem. Geophys. Geosyst.*, ***12*** (8), Q08005–. http://dx.doi.org/10.1029/2010GC003353.

Gardner, W.P., G. Hammond, and P. Lichtner (2013), High performance simulation of multiple environmental tracers: Exploring groundwater age and tracer systematics in high resolution, heterogeneous domains, *Groundwater, in press*.

Goode, D.J. (1996), Direct simulation of groundwater age, *Water Resour. Res.,* ***32*** (2), 289–296.

Hammond, G.E., P.C. Lichtner, and R.T. Mills (2012), *Ebook: Groundwater Reactive Transport Models*, Chapter: PFLOTRAN: Reactive flow and transport code for use on laptops to leadership-class supercomputers, Bentham Science Publishers, pp. 141–159.

Hill, M.C., and C.R. Tiedeman (2007), *Effective Groundwater Model Calibration—With Analysis of Data, Sensitivities, Predictions and Uncertainty*: Hoboken, N.J., Wiley, 464 p.

Hunt, R.J., J. Doherty, and M.J. Tonkin (2007), Are models too simple? Arguments for increased parameterization, Ground Water, 45: 254–262. doi: 10.1111/j.1745-6584.2007.00316.x.

Kaufman & Libby 1954Kaufman, S. & Libby, W. F. (1954), 'The natural distribution of tritium', Phys. Rev. 93, 1337–1344.

Larocque et al. 2009Larocque, M., Cook, P. G., Haaken, K. & Simmons, C. T. (2009), 'Estimating flow using tracers and hydraulics in synthetic heterogeneous aquifers', Ground Water 47(6), 786–796.

Maloszewski & Zuber 1996Maloszewski, P. & Zuber, A. (1996), 'Lumped parameter models for the interpretation of environmental tracer data', IAEA Technical Report .

McCallum, J.L., P.G. Cook, C.T. Simmons, and A.D. Werner (2013), Bias of apparent tracer ages in heterogeneous environments, *Groundwater*, doi: 10.1111/gwat.12052.

Murphy, S., T. Ouellon, J.-M. Ballard, R. Lefebvre, and I. Clark (2011), Tritium-helium groundwater age used to constrain a groundwater flow model of a valley-fill aquifer contaminated with trichloroethylene (Quebec, Canada), *Hydrogeology Journal* ***19***, 195–207. 10.1007/s10040-010-0662-5. http://dx.doi.org/10.1007/s10040-010-0662-5.

Portniaguine, O. and D.K. Solomon (1998), Parameter estimation using groundwater age and head data, Cape Cod, Massachusetts, Water Resour. Res., 34 (4), 637–645. http://dx.doi.org/10.1029/97WR03361.

Pohll, G., Warwick, J. & Benson, D. (2000), 'On the errors associated with two-dimensional stochastic solute transport models', Transport in Porous Media 40(3), 281–293.

Plummer et al. 2004Plummer, L. N., Bexfield, L. M., Anderholm, S. K., Sanford, W. E. & Busenberg, E. (2004), 'Hydrochemical tracers in the middle Rio Grande Basin, USA: 1. Conceptualization of groundwater flow', Hydrogeology Journal 12, 359–388.

RamaRao, B. S., A. M. LaVenue, G. De Marsily, and M. G. Marietta (1995), Pilot point methodology for automated calibration of an ensemble of conditionally simulated transmissivity fields: 1. Theory and computational experiments, *Water Resour. Res.*, ***31*** (3), 475–493, doi:10.1029/94WR02258.

Sanford, W. (2011), Calibration of models using groundwater age, *Hydrogeology Journal*, **19**, 13–16. 10.1007/s10040-010-0637-6. http://dx.doi.org/10.1007/s10040-010-0637-6.

Sanford, W.E., L.N. Plummer, D.P. McAda, L.M. Bexfield, and S.K. Anderholm (2004), Hydrochemical tracers in the middle Rio Grande Basin, USA: 2. Calibration of a groundwater-flow model, Hydrogeology Journal, 12, 389–407. 10.1007/s10040-004-0326-4. http://dx.doi.org/10.1007/s10040-004-0326-4.

Solomon, D.K., D.P. Genereux, L.N. Plummer, and E. Busenberg (2010), Testing mixing models of old and young groundwater in a tropical lowland rain forest with environmental tracers, *Water Resour. Res.* ***46*** (4), W04518–. http://dx.doi.org/10.1029/2009WR008341.

Spalding 1958Spalding, D. (1958), 'A note on mean residence-times in steady flows of arbitrary complexity', Chemical Engineering Science 9(1), 74 – 77.

Tonkin, M., J. Doherty, and C. Moore (2007), Efficient nonlinear predictive error variance for highly parameterized models, *Water Resour. Res.*, ***43***, *W07429, doi:*10.1029/2006WR005348.

Troldborg, L., K.H. Jensen, P. Engesgaard, J.C. Refsgaard, and K. Hinsby (2008), Using environmental tracers in modeling flow in a complex shallow aquifer system., Journal of Hydrologic Engineering, 13 (11), 1037 – 1048.

Varni & Carrerra 1998Varni, M. & Carrerra, J. (1998), 'Simulation of groundwater age distributions.', Water Resources Research 34(12), 3271–3281.

Vecchia, A.V. and R.L. Cooley (1987), Simultaneous confidence and prediction intervals for nonlinear regression models with application to a groundwater flow model, *Water Resour. Res.*, ***23*** (7), 1237–1250, *doi:*10.1029/WR023i007p01237.

Weissmann, G.S., Y. Zhang, E.M. LaBolle, and G.E. Fogg (2002), Dispersion of groundwater age in an alluvial aquifer system, *Water Resour. Res.,* ***38*** (10), 1198–. http://dx.doi.org/10.1029/2001WR000907.

Zhao, X., T.L.B. Fritzel Hernan, A.M. Quinodoz, C.M. Bethke and T. Torgersen (1998), Controls on the distribution and isotopic composition of helium in deep ground-water flows, *Geology,* ***26*** (4), 291–294. http://geology.gsapubs.org/cgi/content/abstract/26/4/291.

APPENDIX A:

The table below contains the environmental tracer concentrations expected in recharge of groundwater at sea level with a mean annual temperature of 20^{o}C. They were calculated assuming no addition of excess air during recharge.

Table 3 - Tracer concentrations in recharge to the groundwater model.

Year	CFC11 (mol/kg)	^{39}Ar (mol/kg)	^{3}H (mol/kg)	^{3}He (mol/kg)
1940	1.35E-16	1.02E-20	3.04E-15	2.83E-15
1941	2.02E-16	1.02E-20	3.04E-15	2.83E-15
1942	2.53E-16	1.02E-20	3.04E-15	2.83E-15
1943	3.03E-16	1.02E-20	3.04E-15	2.83E-15
1944	4.38E-16	1.02E-20	3.04E-15	2.83E-15
1945	6.07E-16	1.02E-20	3.04E-15	2.83E-15
1946	9.61E-16	1.02E-20	3.04E-15	2.83E-15
1947	1.42E-15	1.02E-20	3.04E-15	2.83E-15
1948	2.66E-15	1.02E-20	3.04E-15	2.83E-15
1949	5.01E-15	1.02E-20	3.04E-15	2.83E-15
1950	7.79E-15	1.02E-20	3.35E-14	2.83E-15
1951	1.04E-14	1.02E-20	4.97E-15	2.83E-15
1952	1.59E-14	1.02E-20	1.62E-14	2.83E-15
1953	2.47E-14	1.02E-20	1.34E-14	2.83E-15
1954	3.38E-14	1.02E-20	5.73E-14	2.83E-15
1955	4.17E-14	1.02E-20	6.00E-14	2.83E-15
1956	5.50E-14	1.02E-20	1.63E-14	2.83E-15
1957	7.26E-14	1.02E-20	2.36E-14	2.83E-15
1958	8.58E-14	1.02E-20	1.09E-13	2.83E-15
1959	9.59E-14	1.02E-20	3.27E-13	2.83E-15
1960	1.15E-13	1.02E-20	1.73E-13	2.83E-15
1961	1.44E-13	1.02E-20	9.61E-14	2.83E-15
1962	1.74E-13	1.02E-20	6.48E-14	2.83E-15
1963	2.01E-13	1.02E-20	3.46E-14	2.83E-15
1964	2.44E-13	1.02E-20	2.35E-14	2.83E-15
1965	3.04E-13	1.02E-20	2.41E-14	2.83E-15
1966	3.59E-13	1.02E-20	2.27E-14	2.83E-15
1967	4.04E-13	1.02E-20	2.16E-14	2.83E-15
1968	4.74E-13	1.02E-20	9.80E-15	2.83E-15
1969	5.73E-13	1.02E-20	1.03E-14	2.83E-15
1970	6.64E-13	1.02E-20	1.13E-14	2.83E-15
1971	7.64E-13	1.02E-20	8.64E-15	2.83E-15
1972	8.78E-13	1.02E-20	6.52E-15	2.83E-15
1973	1.01E-12	1.02E-20	8.34E-15	2.83E-15
1974	1.14E-12	1.02E-20	8.55E-15	2.83E-15
1975	1.28E-12	1.02E-20	5.38E-15	2.83E-15
1976	1.41E-12	1.02E-20	6.27E-15	2.83E-15
1977	1.51E-12	1.02E-20	6.26E-15	2.83E-15
1978	1.61E-12	1.02E-20	5.18E-15	2.83E-15
1979	1.69E-12	1.02E-20	5.40E-15	2.83E-15
1980	1.77E-12	1.02E-20	4.43E-15	2.83E-15
1981	1.85E-12	1.02E-20	3.52E-15	2.83E-15
1982	1.94E-12	1.02E-20	4.49E-15	2.83E-15
1983	2.03E-12	1.02E-20	4.33E-15	2.83E-15
1984	2.12E-12	1.02E-20	4.24E-15	2.83E-15
1985	2.24E-12	1.02E-20	4.90E-15	2.83E-15
1986	2.35E-12	1.02E-20	4.26E-15	2.83E-15
1987	2.49E-12	1.02E-20	4.15E-15	2.83E-15

1988	2.60E-12	1.02E-20	2.37E-15	2.83E-15
1989	2.68E-12	1.02E-20	2.14E-15	2.83E-15
1990	2.73E-12	1.02E-20	2.20E-15	2.83E-15
1991	2.75E-12	1.02E-20	2.04E-15	2.83E-15
1992	2.77E-12	1.02E-20	1.85E-15	2.83E-15
1993	2.77E-12	1.02E-20	2.45E-15	2.83E-15
1994	2.77E-12	1.02E-20	2.43E-15	2.83E-15
1995	2.76E-12	1.02E-20	2.07E-15	2.83E-15
1996	2.74E-12	1.02E-20	2.52E-15	2.83E-15
1997	2.72E-12	1.02E-20	2.28E-15	2.83E-15
1998	2.70E-12	1.02E-20	1.76E-15	2.83E-15
1999	2.67E-12	1.02E-20	1.76E-15	2.83E-15
2000	2.67E-12	1.02E-20	1.76E-15	2.83E-15
2001	2.64E-12	1.02E-20	1.76E-15	2.83E-15
2002	2.61E-12	1.02E-20	1.76E-15	2.83E-15
2003	2.58E-12	1.02E-20	1.76E-15	2.83E-15
2004	2.56E-12	1.02E-20	1.76E-15	2.83E-15
2005	2.54E-12	1.02E-20	1.76E-15	2.83E-15
2006	2.51E-12	1.02E-20	1.76E-15	2.83E-15
2007	2.49E-12	1.02E-20	1.76E-15	2.83E-15
2008	2.49E-12	1.02E-20	1.76E-15	2.83E-15
2009	2.49E-12	1.02E-20	1.76E-15	2.83E-15

Synthetic data from the PFLOTRAN initial run.

Table 4 - Observation data from the synthetic groundwater flow and transport system.

Observation well number	Pressure (Pa)	CFC11 (mol/kg)	^{39}Ar (mol/kg)	^{3}H (mol/kg)	^{3}He (mol/kg)
1	5000307	2.168E-12	9.539E-21	9.016E-16	6.478E-15
2	4994372	4.384E-20	7.276E-21	6.223E-19	3.492E-15
3	4986632	7.465E-20	7.136E-21	4.917E-19	3.493E-15
4	4972131	2.960E-28	6.092E-21	1.632E-20	3.492E-15
5	4966773	1.091E-45	5.024E-21	3.294E-22	3.492E-15
6	4958457	1.000E-45	4.462E-21	2.964E-23	3.492E-15
7	4954880	1.000E-45	4.110E-21	5.631E-24	3.492E-15
8	5000310	2.577E-12	1.001E-20	1.144E-15	3.455E-15
9	4995991	1.865E-12	9.445E-21	8.887E-16	6.838E-15
10	4983207	5.927E-15	8.544E-21	2.730E-16	1.174E-14
11	4971350	1.125E-19	7.692E-21	1.590E-18	3.493E-15
12	4967974	2.785E-29	6.822E-21	1.271E-19	3.492E-15
13	4958081	1.000E-45	5.488E-21	1.331E-21	3.492E-15
14	4954558	1.000E-45	4.887E-21	1.152E-22	3.492E-15
15	4999702	1.676E-12	9.402E-21	1.119E-15	1.078E-14
16	4994379	1.103E-15	8.277E-21	6.336E-17	5.804E-15
17	4984829	3.252E-21	7.418E-21	7.600E-19	3.492E-15
18	4970644	1.029E-38	5.631E-21	2.595E-21	3.492E-15
19	4963476	1.215E-40	4.788E-21	1.074E-22	3.492E-15
20	4958186	1.017E-45	5.471E-21	1.655E-21	3.492E-15
21	4953442	1.000E-45	4.958E-21	1.466E-22	3.492E-15
22	4998938	1.776E-12	9.429E-21	1.062E-15	9.680E-15
23	4987097	7.577E-18	7.838E-21	3.603E-18	3.586E-15
24	4982334	3.287E-20	7.155E-21	6.061E-19	3.492E-15
25	4973268	3.211E-26	6.644E-21	1.107E-19	3.492E-15
26	4960899	2.784E-41	5.859E-21	7.141E-21	3.492E-15

27	4956566	1.000E-45	5.116E-21	4.667E-22	3.492E-15
28	4952814	1.000E-45	4.958E-21	2.344E-22	3.492E-15
29	5000792	2.660E-12	9.895E-21	9.813E-16	3.785E-15
30	4990064	4.284E-16	8.271E-21	3.568E-17	5.048E-15
31	4982474	4.405E-28	6.533E-21	5.532E-20	3.492E-15
32	4968258	2.492E-28	6.638E-21	7.869E-20	3.492E-15
33	4963327	4.350E-39	6.058E-21	1.088E-20	3.492E-15
34	4956986	1.000E-45	4.760E-21	9.980E-23	3.492E-15
35	4952681	1.000E-45	3.528E-21	1.861E-25	3.492E-15
36	5000807	2.677E-12	9.881E-21	9.609E-16	3.823E-15
37	4995292	2.371E-14	8.649E-21	8.978E-16	2.429E-14
38	4984400	1.179E-22	7.211E-21	4.286E-19	3.492E-15
39	4968915	1.004E-41	5.803E-21	4.548E-21	3.492E-15
40	4962428	1.000E-45	4.472E-21	2.007E-23	3.492E-15
41	4956375	1.000E-45	3.651E-21	3.112E-25	3.492E-15
42	4952725	1.000E-45	2.928E-21	3.910E-27	3.492E-15

DISTRIBUTION

1	MS0899	Technical Library	9536 (electronic copy)
1	MS0359	D. Chavez, LDRD Office	1911

Sandia National Laboratories